The nature of ice-nucleating particles affects the radiative properties of tropical convective cloud systems

Rachel E. Hawker*[1], Annette K. Miltenberger[1, a], Jonathan M. Wilkinson[2], Adrian A. Hill[2], Ben J. Shipway[2], Zhiqiang Cui[1], Richard J. Cotton[2], Ken S. Carslaw[1], Paul R. Field[1, 2], Benjamin J. Murray[1].

1. Institute for Climate and Atmospheric Science, University of Leeds, Leeds, LS2 9JT, United Kingdom.
2. Met Office, Exeter, EX1 3PB, United Kingdom.
a. now at : Institute for Atmospheric Physics, Johannes Gutenberg University Mainz, Mainz, 55128, Germany.

Correspondence to: Rachel E. Hawker (eereh@leeds.ac.uk)

Abstract

Convective cloud systems in the maritime tropics play a critical role in global climate, but accurately representing aerosol interactions within these clouds persists as a major challenge for weather and climate modelling. We quantify the effect of ice-nucleating particles (INP) on the radiative properties of a complex Tropical Atlantic deep convective cloud field using a regional model with an advanced double-moment microphysics scheme. Our results show that the domain-mean daylight outgoing radiation varies by up to 18 W m^{-2} depending on the bio- and physico-chemical properties of INP. The key distinction between different INPs is the temperature dependence of ice formation, which alters the vertical distribution of cloud microphysical processes. The controlling effect of the INP temperature dependence is substantial even in the presence of secondary ice production, and the effects of secondary ice formation depend strongly on the nature of the INP. Our results have implications for climate model simulations of tropical clouds and radiation, which currently do not consider a link between INP particle type and ice water content. The results also provide a challenge to the INP measurement community, since we demonstrate that INP concentration measurements are required over the full mixed-phase temperature regime, which covers around 10 orders of magnitude in INP concentration.

1. Introduction

Deep convective clouds are important drivers of local, regional and global climate and weather (Arakawa, 2004; Lohmann et al., 2016). They produce substantial precipitation (Arakawa, 2004) and the associated phase changes release latent heat that helps to drive global atmospheric circulation (Fan et al., 2012). Convective clouds have a direct impact on climate through interactions with incoming shortwave and outgoing longwave radiation (Lohmann et al., 2016), for example by producing radiatively important long-lived cirrus clouds (Luo and Rossow, 2004). The clouds extend from the warmer lower levels of the atmosphere where only liquid exists to the top of the troposphere where only ice exists (Lohmann et al., 2016). Between these levels is the mixed-phase region where both liquid and ice coexist and interact (Seinfeld and Spyros, 2006). Within the mixed-phase region, primary ice particles can form heterogeneously through the freezing of cloud droplets by ice-nucleating particles (INP). The importance and relative contribution of heterogeneous freezing to ice crystal number concentrations (ICNC) and resultant cloud properties, such as cloud reflectivity, is very uncertain (Cantrell and Heymsfield, 2005; Kanji et al., 2017). This uncertainty stems from the difficulty of predicting INP number concentrations (Kanji et al., 2017; Lacher et al., 2018) as well as the difficulty of quantifying complex interactions between heterogeneous freezing and other ice production mechanisms (Crawford et al., 2012; Huang et al., 2017; Phillips et al., 2005).

Understanding the effects of INP on convective clouds presents substantial challenges. Measurements indicate that INP number concentrations can vary by as much as six orders of magnitude at any one temperature (DeMott et al., 2010; Kanji et al., 2017), and large variability exists even in measurements of individual regions or aerosol populations (Boose et al., 2016b; Kanji et al., 2017; Lacher et al., 2018). For example, there are four orders of magnitude variation in summertime measurements of INP number concentrations in the Saharan Air Layer at -33°C (Boose et al., 2016b). Even for particles of similar and known mineralogy, measurements of ice-nucleation efficiency can span several orders of magnitude: The spread in laboratory measurements of ice nucleation active site densities (n_s) for different types of feldspar spans seven orders of magnitude at -15°C (Atkinson et al., 2013; Harrison et al., 2016, 2019). Our ability to understand and quantify such variability in INP concentrations has improved as more measurements have been made. Although meteorological factors are not strong indicators of INP concentrations (Boose et al., 2016a; Lacher et al., 2018), aerosol surface area (Lacher et al., 2018) and diameter (DeMott et al., 2015) provide some predictability and global models based on known INP-active materials show reasonable skill in simulating global INP concentrations (Vergara-Temprado et al., 2017).

57 It is known from model simulations that changes in INP number concentration affect the microphysical properties and

58 behaviour of deep convective clouds (Deng et al., 2018; Fan et al., 2010a, 2010b; Gibbons et al., 2018; Takeishi and

59 Storelvmo, 2018). However, in these model studies perturbations to INP number concentrations have predominantly

60 involved uniform increases in aerosol or INP concentrations with all simulations using the same INP parameterisation

61 (Carrió et al., 2007; Connolly et al., 2006; Deng et al., 2018; Ekman et al., 2007; Fan et al., 2010a; Gibbons et al., 2018;

62 van den Heever et al., 2006; Phillips et al., 2005). Where different INP parameterisations have been used (Eidhammer

63 et al., 2009; Fan et al., 2010b; Liu et al., 2018; Takeishi and Storelvmo, 2018), the results have in most cases been

64 interpreted in terms of the overall increase in INP number concentration (Fan et al., 2010b; Liu et al., 2018; Takeishi

65 and Storelvmo, 2018). However, there are important structural differences between different INP parameterisations

66 that have not yet been explored in detail. For example, currently available and regularly used parameterisations of INP

67 vary substantially in the dependence of INP activity on temperature. We hypothesise that the difference between

68 parameterisations will be particularly important for deep convective clouds because heterogeneous ice formation

69 occurs over a very wide temperature range from just below 0 to around -38°C in the mixed-phase region of these

70 clouds. For the same dust particle concentration, predicted INP concentrations can increase by up to three orders of

71 magnitude from -15 to -20°C (corresponding to approximately 1 km altitude change) using an INP parameterisation

72 with a steep temperature dependence (lower INP concentrations at high temperatures and higher INP concentrations

73 at low temperatures) (Atkinson et al., 2013), but by less than one order of magnitude using an INP parameterisation

74 with a shallower dependence (DeMott et al., 2010; Meyers et al., 1992). We hypothesise that such large differences in

75 ice production rates between INP parameterisations are likely to affect cloud properties. In simulations of deep

76 convective clouds over North America (Takeishi and Storelvmo, 2018) there were differences in the magnitude and

77 altitude of droplet depletion depending on INP parameterisation choice (Bigg, 1953; DeMott et al., 2010, 2015).

78 Uncertainty in mixed-phase cloud properties is compounded further by a lack of quantification of the interaction of

79 heterogeneous freezing with other ice production mechanisms. Ice crystals in the mixed-phase region can also be

80 formed by secondary ice production (SIP) from existing hydrometeors (Field et al., 2017) and droplets can freeze

81 homogeneously below around -33°C (Herbert et al., 2015). In observations of convective clouds with relatively warm

82 cloud-top temperatures (Fridlind et al., 2007; Heymsfield and Willis, 2014; Ladino et al., 2017; Lasher-Trapp et al.,

83 2016; Lawson et al., 2015), ICNC has frequently exceeded INP number concentrations by several orders of magnitude,

84 suggesting that secondary ice production is the dominant small-ice formation mechanism in mixed-phase regions

85 (Ladino et al., 2017). The importance of heterogeneous ice production relative to secondary and homogeneous

86   freezing has therefore been questioned (Ladino et al., 2017; Phillips et al., 2007) and it has been proposed that INP

87   concentrations may only be relevant up to a threshold needed to initiate SIP (Ladino et al., 2017; Phillips et al., 2007),

88   a value that may be as low as 0.01 L^{-1} (Crawford et al., 2012; Huang et al., 2017) for the Hallett Mossop process (Hallett

89   and Mossop, 1974). If this is the case, in clouds where SIP may also be initiated by the primary freezing of a few large

90   (~1 mm) droplets in a rising parcel (Field et al., 2017), INP number concentrations may be largely irrelevant to cloud

91   ice properties. The effect of INP and INP parameterisation on convective cloud properties must therefore be examined

92   with consideration for the presence of, and interactions with, SIP.

93   Here we explore how the choice of INP parameterisation affects the properties of a large and realistic cloud field

94   containing clouds at all levels as well as deep convective systems in the eastern Tropical Atlantic with a focus on the

95   top of atmosphere (TOA) outgoing radiation. The eastern Tropical Atlantic is an ideal location in which to examine the

96   role of INP concentrations in convective cloud systems because, owing to its position at the interface between the

97   Saharan Air Layer and the Inter Tropical Convergence Zone, it is subject to both high levels of convective activity and

98   high loadings of desert dust, a relatively well-defined INP type (DeMott et al., 2003; Niemand et al., 2012; Price et al.,

99   2018). First, we determine how the presence of INP alters the radiative properties of the cloud field. We then

100   examine how the properties of the simulated cloud field, including cloud shortwave reflectivity, cloud fraction and

101   anvil extent, depend on the choice of INP parameterisation. In particular, we examine the importance of the

102   dependence of INP number concentration on temperature, referred to as INP parameterisation slope herein, as a

103   major factor that determines cloud properties.

104

2. Methods

2.1.   Model set-up

2.1.1 Regional domain and initial conditions

107   Simulations described in this article were performed using the Unified Model (UM) version 10.8 (GA6 configuration)

108   (Walters et al., 2017). The UM is a numerical weather prediction model developed by the UK Met Office. We use a

109   regional nest within the global model simulation, which has a grid spacing of 1 km (900*700 grid points) and 70

110   vertical levels. Meteorology of the driving global model is based on operational analysis data. Within the nested

111   domain, the Cloud AeroSol Interacting Microphysics scheme (CASIM) is employed to handle cloud microphysical

113   properties. The Met Office global model is used to initialise the nested simulation at 00:00 on the 21st of August 2015

114   and is used throughout the simulation for the boundary conditions.

115   The 21st of August 2015 was chosen for simulation to coincide with flight b933 of the Ice in Clouds Experiment – Dust

116   (ICE-D) July-August 2015 field campaign that targeted convective clouds extending to and beyond the freezing level.

117   The aerosol profile measured during flight b933 (Fig. A1a) was used to derive the aerosol profiles prescribed over the

118   nested domain at the beginning of the simulation and are constantly applied at the boundaries. Model profiles were

119   calculated as follows: The UM vn 10.3 was used to simulate a domain comprising the entire Tropical Atlantic and West

120   Africa. This simulation was initiated on the 18th August 2015 with a grid spacing of 8 km using the UM operational one-

121   moment microphysics (i.e. not CASIM) and the CLASSIC aerosol scheme with a 6-bin dust model(Johnson et al.,

122   2015a). On the day of the b933 flight (21st August 2015), a dust layer was present between 2 and 3 km altitude.

123   Comparison to MODIS AOD data indicates agreement between the model and observations (not shown). This UM vn

124   10.3 simulation was used to calculate the average dust profile (mass and number concentration) over the CASIM

125   domain on the 21st of August 2015 and these dust profiles are applied in the nested domain as the insoluble aerosol

126   profiles (Fig. A1a). The approximate difference between the dust aerosol profile provided by the UM regional

127   simulation and the observed aerosol profile measured during flight b933 (comprising both insoluble and soluble

128   particles) is used as the soluble aerosol profile (Fig. A1a). The simulations are 24 hours in length.

129   **2.1.2. CASIM microphysics**

130   CASIM is a multi-moment bulk scheme, which is configured to be two-moment in this work. Both number

131   concentration and mass concentration for each of the five hydrometeor classes (cloud droplets, rain droplets, ice

132   crystals, graupel, snow) are prognostic variables. The model set-up is very similar to that used in Miltenberger et al.

133   (2018) including the parameter choices within CASIM. CASIM has been used and tested previously in simulations of

134   coastal mixed-phase convective clouds (Miltenberger et al., 2018), South-East Pacific stratocumulus clouds (Grosvenor

135   et al., 2017), Southern Ocean supercooled shallow cumulus (Vergara-Temprado et al., 2018), midlatitude cyclones

136   (McCoy et al., 2018) and CCN-limited Arctic clouds (Stevens et al., 2018).

137   Cloud droplet activation is parameterised according to (Abdul-Razzak and Ghan, 2000). The soluble accumulation

138   mode aerosol profile shown in Fig. A1a is used for cloud droplet activation and a simplistic CCN activation

139   parameterisation is included for the insoluble aerosol mode(Abdul-Razzak and Ghan, 2000) that assumes a 5% soluble

140   fraction on dust. Scavenging is not represented. Collision-coalescence, riming of ice crystals to graupel and

141   aggregation of ice crystals to snow is represented. Rain drop freezing is described using the parameterisation of Bigg

142   (1953). For reference, the modelled domain-mean out-of-cloud temperature and relative humidity are shown in Fig.

143   A1b. The model time-step is 5 seconds.

144   Heterogeneous ice nucleation is represented using 5 different parameterisations: Cooper (1986) (C86), Meyers et al.

145   (1992) (M92), DeMott et al. (2010b) (D10), Niemand et al. (2012) (N12) and Atkinson et al. (2013) (A13) (Fig. 1). C86

146   and M92 calculate a freezing rate based on temperature and are independent of aerosol concentration. D10

147   calculates an INP concentration from temperature and the concentration of insoluble aerosol with a diameter greater

148   than 0.5 μm. N12 and A13 calculate an INP concentration from the temperature dependent active surface site density

149   and the surface area of insoluble aerosol (n_s). For A13, a potassium-feldspar fraction of 0.25 is assumed. This is the

150   upper recommended fraction(Atkinson et al., 2013) which was deemed appropriate because of the study region's

151   exposure to Saharan dust outflow. M92 is described as a deposition and condensation freezing parameterisation

152   (Meyers et al., 1992) and is often used alongside an immersion freezing parameterisation in modelling studies (Deng

153   et al., 2018; Fan et al., 2010b, 2010a; Gibbons et al., 2018). However, the M92 parameterisation is based on aircraft

154   continuous flow diffusion chamber measurements and those measurements should capture all relevant nucleation

155   mechanisms (see Vali et al., 2015). To represent nucleation at conditions relevant for clouds with liquid water present,

156   we have set the saturation term in the M92 parameterisation to water saturation. One simulation is conducted with

157   no active heterogeneous ice nucleation representation (NoINP). The INP parameterisations inspect the conditions and

158   aerosol concentrations within a gridbox and use that information to predict an ice production rate via heterogeneous

159   freezing. The supercooled droplets are depleted by the freezing parameterisation, but scavenging of INPs is not

160   represented. Homogeneous freezing of cloud droplets is parameterised according to Jeffery and Austin (1997).

161   Secondary ice production (SIP) is represented using an approximation of the Hallett Mossop process which occurs

162   between -2.5 and -7.5°C. The efficiency of the Hallett Mossop process increases from -2.5 and -7.5°C to 100% at -5°C.

163   The rate of splinter production per rimed mass is prescribed with 350 new ice splinters produced per milligram of rime

164   at -5°C. The ice splinters produced by the representation of the Hallett Mossop process are the smallest allowable size

165   of ice in the model (i.e. 10^{-18} kg). The rate of splinter production by the Hallett Mossop process is based on the best

166   available estimate of the efficacy of the mechanism (Connolly et al., 2006; Hallett and Mossop, 1974; Mossop, 1985).

167   In-situ cloud observations have frequently observed ICNC that could be explained by the Hallett Mossop process, but

168   the mechanism underlying the Hallett Mossop process as well as the ice particle production rate remain uncertain and

169   not well quantified (Field et al., 2017). A maximum splinter production rate of 350 per milligram of rimed material has

170   been measured in a number of laboratory studies (Hallett and Mossop, 1974; Mossop, 1985) and has been applied as

171   the best estimate here and in previous modelling studies (Connolly et al., 2006), although other rates have also been

172   measured (Heymsfield and Mossop, 1984; Saunders and Hosseini, 2001). Uncertainties regarding the rate of splinter

173   production by Hallett Mossop are an important consideration that will be investigated in future work; this study

174   explores the structural uncertainty of the presence/absence of the Hallett Mossop process as currently understood.

175   Other mechanisms of SIP such as collision fragmentation, droplet shattering and sublimation fragmentation have

176   been proposed (Field et al., 2017), but are not represented in these simulations, in part because they are very poorly

177   defined and it is not clear how important they are. Other studies have attempted to model some of these additional

178   SIP processes (Phillips et al., 2018; Sullivan et al., 2018) but that was beyond the scope of this study.

179   **2.1.3. Cloud radiation**

180   The radiative processes are represented by the Suite of Community RAdiative Transfer codes based on Edwards and

181   Slingo (SOCRATES) (Edwards and Slingo, 1996; Manners et al., 2017), which considers cloud droplet number and mass,

182   as well as ice crystal and snow water paths for the calculation of cloud radiative properties. It does not respond to

183   changes in ice crystal or snow number concentration, or any changes to rain or graupel species. The cloud droplet

184   single scattering properties are calculated from the cloud droplet mass and effective radius in each gridbox using the

185   equations detailed in Edwards and Slingo (1996). Snow and ice are combined to form one ice category for the

186   purposes of the radiation calculations. The single scattering properties of this snow and ice category are calculated

187   from their combined mass and the ambient temperature. The parameterisation of bulk optical properties of snow and

188   ice used in the model is detailed in Baran et al. (2014).

189   The radiative properties (shortwave, longwave and total radiation) are calculated for daylight hours only, i.e. 10:00-

190   17:00 UTC. For all other modelled properties presented, except when plotted against a corresponding radiative

191   property, values are calculated for the last 14 hours of the simulation, i.e. from 10:00 - 24:00. The sensitivity of

192   analysis to time period selection was tested and found to have little impact.

193   Changes to outgoing radiation from cloudy regions and changes in cloud fraction both contribute to the total overall

194   change in outgoing radiation between two simulations. The contributions from changes in outgoing radiation from

195   cloudy regions and cloud fraction to the overall radiative differences between simulations were calculated separately

196   as described below. The cloudy regions contribution (ΔRad_{REFL}) to a domain radiative difference between two

197   simulations s and r (s − r) is calculated using Eq. (1).

198 $$\Delta Rad_{REFL} = cf_r \times \Delta Rad_{cl} \qquad (1)$$

199 where cf_r is the cloud fraction of simulation r and ΔRad_{cl} is the change in outgoing radiation from cloudy areas only

200 between simulations (s − r). The cloud fraction contribution (ΔRad_{CF}) is calculated using Eq. (2).

201 $$\Delta Rad_{CF} = \left(Rad_{r,cl} - Rad_{r,cs}\right) \times \Delta cf \qquad (2)$$

202 Where $Rad_{r,cl}$ is the mean outgoing radiation from cloudy regions in simulation r and $Rad_{r,cs}$ is the mean outgoing

203 radiation from clear sky regions in simulation r and Δcf is the difference in cloud fraction between simulations s and r

204 (s-r). There is interaction between the outgoing radiation from cloudy regions and cloud fraction changes (ΔRad_{INT})

205 which is calculated in Eq (3).

206 $$\Delta Rad_{INT} = \Delta Rad_{cl} \times \Delta cf + \Delta Rad_{cs} \times (1 - cf_s) \qquad (3)$$

207 Where ΔRad_{cs} is the change in mean outgoing radiation from clear sky areas between simulations s and r and cf_s is

208 the cloud fraction of simulation s.

209 The total outgoing radiation difference between simulations s and r (ΔRad_{s-r}) is therefore as shown in Eq. (4).

210 $$\Delta Rad_{s-r} = Rad_s - Rad_r = \Delta Rad_{REFL} + \Delta Rad_{CF} + \Delta Rad_{INT} \qquad (4)$$

211 The interaction term ΔRad_{INT} was found to be negligible and was therefore ignored for the purpose of this paper.

212 **2.1.4. Model simulations**

213 The conducted simulations are as follows:

214   -   Five simulations with different heterogeneous ice nucleation parameterisations (C86, M92, D10, N12 and

215   A13) with a representation of the Hallett Mossop process (SIP_active).

216   -   One simulation with no heterogeneous ice nucleation (NoINP), but with a representation of the Hallett

217   Mossop process (SIP_active).

218   -   Five simulations with different heterogeneous ice nucleation parameterisations (C86, M92, D10, N12 and

219   A13) without a representation of the Hallett Mossop process (SIP_inactive).

220 The INP number concentration ([INP]) predicted by the five INP parameterisations (C86, M92, D10, N12, A13) are

221 compared with the available measurements from the study region (Price et al., 2018; Welti et al., 2018) in Fig. 1,

222   including those taken during the ICE-D field campaign (Price et al., 2018). All parameterisations are in reasonable

223   agreement with the measurements (and with each other) at around -17°C, but deviate strongly at higher and lower

224   temperatures. Importantly, the INP parameterisation slopes of the chosen parameterisations span the range used

225   within regional models (from a shallow $\mathrm{dlog_{10}[INP]}/\mathrm{d}T$ = -0.07 in M92 (Meyers et al., 1992) to a steep $\mathrm{dlog_{10}[INP]}/\mathrm{d}T$ =

226   -0.45 in A13 (Atkinson et al., 2013)).

227   When analysing the simulation output, cloudy grid boxes were classed as those containing more than 10^{-5} kg kg^{-1}

228   condensed water from cloud droplets, ice crystals, graupel and snow. Rain was not included to ensure analysis did not

229   include areas below cloud base. Other cloud thresholds were tested and found to have no notable effect on the

230   results. For cloud categorisation into low, mid and high clouds, model vertical columns containing cloudy grid boxes

231   were categorised by cloud altitude. Low cloud occurs below 4km, mid cloud between 4 and 9 km and high cloud above

232   9 km. Columns with cloudy grid boxes in two or more cloud categories were classified as mixed category columns

233   according to the vertical placement of the cloudy grid boxes, e.g. low/high for columns containing cloud below 4 km

234   and above 9 km. 4 and 9 km were chosen as the low/mid and mid/high division points because they are just below

235   two well-defined peaks in cloud base heights (not shown) and roughly correspond to the beginning of the

236   heterogeneous and homogeneous freezing regions, respectively.

2.2.   The observed case

238   MODIS visible images of the 21st August 2015 are shown in Fig. 2 (a, b) alongside a time series of snapshots of the TOA

239   outgoing longwave radiation in our one of our simulations (c - h). The simulated cloud field has more cloud-free areas

240   than the satellite images but in general produces clouds similar to those shown in the satellite image and in

241   approximately the correct location. Overall the simulations produce a complex and realistic cloud field. Snapshots of

242   the simulated model TOA outgoing shortwave radiation are shown in Fig. A2.

243   In-situ measurements of cloud and aerosol properties were made using the UK FAAM Bae-146 research aircraft, which

244   was flown from Praia, Cape Verde Islands. An extensive suite of in-situ aerosol and cloud particle instruments were

245   operated onboard the aircraft and are described in detail in Lloyd et al. (2019). The aircraft penetrated the growing

246   convective clouds at a range of altitudes from just below the freezing level up to -20°C. In order to show that the

247   model reproduces the observed conditions, the observational data were compared to the conditions in modelled

248   clouds of similar size to those the aircraft flew in (10 − 150 km^2) where a comparison was thought appropriate.

249   Comparisons of a selection of simulated cloud properties with aircraft data are shown in Fig. A3. In-cloud

250   measurements from the aircraft were selected using the same total water content threshold as for the model data

251   (10^{-5} kg kg^{-1}). Note that observational data only samples clouds along the 1D flight path, while model results include all

252   grid points inside the selected clouds.

253   The vertical wind and cloud droplet and ice number concentrations are shown Fig. A3. The vertical wind speeds from

254   the model and aircraft measurements agree well (Fig. A3a). The aircraft data exhibit less measurements of vertical

255   wind speeds above 10 m s^{-1} but that is expected since the aircraft was purposefully not flow in very high updraft

256   speeds. The aircraft cloud droplet number concentration (CDNC), measured using a DMT cloud droplet probe, falls

257   predominantly in the regions of parameter space most highly populated by model data when plotted against vertical

258   wind speed (Fig. A3b). Note that the simulated points in Figure A1b represent values of CDNC and updraft speed in all

259   cloudy gridboxes, not just those at cloud base. The updraft speed is collocated with CDNC and therefore does not

260   necessarily represent the updraft speed at which the cloud droplets were activated. The higher CDNC values exhibited

261   in the model data may be due to the higher updraft speeds which were not measured by the aircraft. The observed

262   ICNC was derived from measurements using the DMT Cloud Imaging Probes (CIP-15 and CIP-100) and the SPEC

263   Stereoscopic optical array probe covering a size range from 10 to 6200 µm using the SODA2 processing code to

264   reconstruct ice particle images that are fully contained within the probe sample volume. Because of uncertainties in

265   the optical array probe sample volume for very small images, only ice particle images greater than 100 µm were

266   included. The aircraft ICNC fall almost entirely within the range of the model values (Fig. A3c).

267

3. Results

3.1.   Effect of INP and INP parameterisation on outgoing radiation

270
271   We first examine the effect of INP parameterisation on the outgoing radiation relative to the simulation where the

272   only source of primary ice production was through homogeneous freezing (NoINP). When contrasting the effect of

273   different INP parameterisations in Sect 3.1-3.4, the Hallett Mossop process was always active. As stated in Sect. 2.1.3,

274   the radiation code is represented by the Suite Of Community RAdiative Transfer codes based on Edwards and Slingo

275   (SOCRATES) (Edwards and Slingo, 1996; Manners et al., 2017), and responds to changes in cloud droplet number and

276   cloud droplet, ice crystal and snow mass. The results detailed below relate to either the domain-wide properties or all

277   in-cloud regions within the domain. This means that the results describe the direct and indirect changes occurring due

278   to INP across all cloud present in the domain, including low-level liquid clouds, mixed-phase clouds without a

279   convective anvil and very deep convective clouds with an anvil. The effects of INP parameterisation and SIP on

280   convective anvils are discussed in Sect. 3.4.

281   Domain-mean TOA outgoing radiation (daylight hours, shortwave plus longwave) is enhanced by the inclusion of INP

282   in all cases (Fig. 3a). The enhancement in outgoing radiation varies between 2.6 W m^{-2} for D10 and 20.8 W m^{-2} for A13

283   relative to the NoINP simulation. There is a variation of up to 18.2 W m^{-2} depending on the chosen representation of

284   heterogeneous ice nucleation, which shows that the INP parameterisation can affect outgoing radiation as much as

285   excluding or including heterogeneous freezing altogether. Radiative changes from the NoINP simulation due to the

286   inclusion of INP are caused mainly by changes to outgoing shortwave radiation. The inclusion of INP enhances

287   outgoing shortwave radiation by between 5.3 W m^{-2} for D10 and 26.6 W m^{-2} for A13 (Fig. A4a). Differences in outgoing

288   longwave radiation are comparatively small (-2.7- W m^{-2} for D10 to -5.8 W m^{-2} for A13; Fig. A4b) due to similar cloud

289   top heights between simulations of these thermodynamically limited clouds. Bear in mind that SIP was active

290   (SIP_active) in the simulations summarised in Fig. 3a, indicating that these cloud systems are sensitive to INP even in

291   the presence of SIP. This is consistent with a comparatively small change in TOA radiation when SIP is active relative to

292   when it is inactive (Fig. 3b and 3c) (we discuss the role of SIP in more detail in Sect. 3.5).

293   The slope of the INP parameterisation is a key determinant of the outgoing radiation. There is a statistically significant

294   correlation between INP parameterisation slope and total TOA outgoing radiation ($r^2 = 0.75$, $p < 0.01$, $n = 10$) (Fig. 3c).

295   Changes in outgoing radiation due to the presence of INP are caused by a combination of changes to the outgoing

296   radiation from cloudy regions, caused by changes in cloud structure and microphysical properties, and changes to

297   domain cloud fraction, whose contributions to the total radiative difference are shown in Fig. 3a (left and centre). In

298   order to appreciate the reasons for these trends, we will now take a closer look at the effect of INP on outgoing

299   radiation from cloudy regions only, domain cloud fraction and cloud type.

300   **3.2.   Effect of INP and INP parameterisation on outgoing radiation from cloudy regions**

301   Here we discuss the changes in outgoing radiation from cloudy regions only due to INP parameterisation choice.

302   Daytime outgoing radiation from cloudy regions increases due to INP for all but one INP parameterisation (Fig. 4a).

303   The absolute change in outgoing radiation from cloudy regions is between –0.8 (D10) and +28.1 (A13) W m^{-2}, and the

304   larger values are a result of large increases in reflected shortwave (up to +37.2 W m^{-2}) and relatively moderate

305   decreases in outgoing longwave radiation (up to –11.1 W m^{-2}) from cloudy regions. The above absolute changes in

306   outgoing radiation from cloudy regions contribute between –0.7 and +11.4 W m^{-2} to the domain-mean change in

307   outgoing radiation due to the presence of INP (Fig. 3a, cloudy regions contribution).

308   The enhancement of outgoing radiation from cloudy regions due to INP is caused primarily by increases in cloud

309   condensate relative to the NoINP simulation (Fig. 4b). When INP are included in a simulation, snow and cloud droplet

310   water path are enhanced, causing increases in total cloud condensate, despite decreases (in all except A13) in ice

311   crystal water path. Snow, cloud droplets and ice crystals are the hydrometeors that affect outgoing radiation in CASIM

312   and the combined water path of these three species is significantly positively correlated with cloud shortwave

313   reflectivity (r^2 = 0.62, p < 0.01, n = 11) (Fig. 4c). The mechanism for this INP induced increase in cloud condensate and

314   consequently cloud shortwave reflectivity is as follows: When heterogeneous ice nucleation is active, liquid is

315   consumed in the warmer regions of mixed-phase clouds because of increased heterogeneous ice nucleation (Fig. 1)

316   and SIP (Fig. A5a). The resultant additional ice crystals in mixed-phase regions facilitate riming causing increases in

317   snow and graupel (Fig. A5c, d), increasing snow water path and reflectivity in mixed-phase and ice clouds. At the same

318   time, the enhanced production of relatively heavy snow and graupel increases precipitation which on evaporation

319   below 4 km, reduces out-of-cloud temperature and increases relative humidity (Fig. A6a, b). This leads to increases in

320   water path in low-level liquid clouds and thus an enhancement in their shortwave reflectivity.

321   However, increases in total cloud condensate alone cannot account for the differences in outgoing radiation from

322   cloudy regions between simulations using different INP parameterisations, which are caused by a combination of

323   cloud microphysical responses. We find that outgoing radiation from cloudy regions is significantly negatively

324   correlated with INP parameterisation slope (r^2 = 0.63, p < 0.01, n = 10) (Fig. 5a), i.e. simulations using a steep INP

325   parameterisation have a higher outgoing radiation from cloudy regions. This result makes sense when we consider the

326   relationships between INP parameterisation slope and a multitude of cloud microphysical properties affecting cloud

327   radiative properties. In particular, a steep INP parameterisation results in a mixed-phase cloud region characterised by

328   a higher ice crystal water path aloft (r^2 = 0.80, p < 0.01, n = 10; Fig. 5b) and higher cloud droplet number

329   concentrations at the bottom of the mixed-phase region (r^2 = 0.89, p < 0.01, n = 10; Fig. 5c) when compared to

330   shallower parameterisations. A steeper INP parameterisation slope allows increased transport of liquid to upper cloud

331   levels due to lower rates of heterogeneous freezing (Fig. 1) and SIP at high temperatures (Fig. A5a). This, combined

332   with higher INP concentrations at low temperatures (Fig. 1), increases ICNC at upper mixed-phase altitudes, as well as

333   enhancing the lifetime of liquid cloud droplets at lower altitudes in the mixed-phase region when compared to

334   shallower INP parameterisations.

3.3.   Effect of INP and INP parameterisation on cloud fraction

336   Overall cloud fraction is increased by INP for all INP parameterisations and these increases in cloud fraction contribute

337   about as much to changes in domain-mean radiation as the changes in outgoing radiation from cloudy regions (Fig. 3a,

338   cloud fraction contribution). Increases in domain cloud fraction due to INP are driven by cloud cover increases in the

339   warm and mixed-phase regions of the cloud (~ 4 -6 km), offset somewhat by decreases in the homogeneous freezing

340   regime (~ 10 - 14 km) (Fig. 6a). Cloud fraction increases at mid-levels occur because heterogeneous ice nucleation

341   induces an increase in precipitation-sized particles (snow and graupel) which sediment to lower levels and moisten the

342   atmosphere by evaporation (Fig. A6a, b). This increases new cloud formation and may prolong the lifetime of existing

343   cloud cells. Additionally, increased droplet freezing and riming in the mixed-phase cloud region releases latent heat

344   and invigorates cloud development with increases in updraft speed just above 4 km (Fig. A6c). The increased cloud

345   fraction at mid-levels due to INP are partially offset by a reduced cloud fraction above 10 km (Fig. 6a) which is caused

346   by an INP induced enhancement in freezing and riming in the mixed-phase region reducing moisture transport to the

347   homogeneous freezing regime.

348   The effects of INP on the altitude profile of cloud fraction are strongest for shallow INP parameterisation slopes, which

349   have a freezing profile most different to that of the NoINP simulation (Fig. 6a). At 5 km, the shallowest

350   parameterisation (M92) causes the largest increase in cloud fraction, while the steepest parameterisation (A13)

351   causes the smallest (r^2 = 0.83, p < 0.05, n = 5). At 12 km, the order is reversed, and steep parameterisations exhibit the

352   highest cloud fraction (r^2 = 0.94, p < 0.01, n = 5). The largest cloud fraction-induced increases in outgoing radiation

353   relative to the NoINP simulation (Fig. 3a) are seen in simulations using steeper INP parameterisations because these

354   simulations exhibit higher cloud fractions at high altitudes (~12 km), translating into the higher total cloud fraction.

355   These slope dependent changes in cloud fraction are explained by a relationship between cloud fraction and several

356   microphysical properties affecting cloud fraction. For example, steeper INP parameterisations produce higher ICNC at

357   the top of the mixed-phase region (10 km) as well as higher ratios of ice crystal mass to snow and graupel mass within

358   the homogeneous freezing region (12 km) (Fig. 6b, c). A higher number and mass of ice crystals relative to those of

359   larger precipitation-sized hydrometeors with the steepest parameterisations results in lower frozen hydrometeor

360   sedimentation, a longer cloud lifetime and a higher cloud fraction.

3.4. Effect of INP and INP parameterisation on cirrus anvils

Our results show that the INP parameterisation affects the properties and spatial extent of cirrus anvils. We define

cirrus anvils to be regions where cloud is present above 9 km only (further details available in Sect. 2.1.4). 2D aerial

images of cloud categorisation (Fig. 7a-f) show well-defined regions of anvil cloud (light blue - H) surrounding a large

convective system containing clouds at a range of altitudes from <4 km to >9 km. There are clearly differences in the

extent and position of cloud categories between simulations (Fig. 7a -f).

The presence of INP reduces convective anvil extent by between 2.1 and 4.1% of the domain area depending on the

choice of INP parameterisation (Fig. 7 g), corresponding to a decrease in anvil cloud of between 22 and 53% relative to

the NoINP simulation (not shown). The reduction in anvil extent in the presence of INP is caused by increased liquid

consumption at all mixed-phase levels, due to heterogeneous freezing, enhanced SIP and increased graupel and snow

production, reducing the availability of cloud droplets for homogeneous freezing (Fig. A5b), reducing ICNC at cloud-

top, and reducing cloud anvil extent (Fig. 7g).

Reductions in anvil extent caused by INP are somewhat offset by the overall increases in cloud fraction across the

domain (Fig. 7g). However, it is possible that the effect of INP and INP parameterisation choice on anvil cloud fraction,

and the contribution of anvil cloud to overall cloud fraction and radiative changes, would become larger with a longer

analysis period. This is because detrained convective anvils can persist longer in the atmosphere than the convective

core that creates them (Luo and Rossow, 2004; Mace et al., 2006), but this is beyond the scope of the current study.

3.5. Importance of secondary ice production

It has been argued that primary ice particle production rate is unimportant for convective cloud properties when

secondary ice production (SIP) is active (Fridlind et al., 2007; Heymsfield and Willis, 2014; Ladino et al., 2017; Lawson

et al., 2015) because primary ice crystal concentrations are often overwhelmed by ice crystals formed via SIP (Field et

al., 2017). However, the results shown in Fig. 3a (in which the simulations included SIP) do not support this argument.

We find that the microphysical and radiative properties of the cloud field depend strongly on the properties of the INP

even with SIP (Hallett-Mossop process) occurs. Furthermore, the effect of including SIP on daylight domain-mean

outgoing radiation varies between –2.0 W m^{-2} and +6.6 W m^{-2} (Fig. 3b), showing that SIP has a smaller effect than the

INP parameterisation. Furthermore, the effect of SIP depends on the INP parameterisation. Therefore, rather than

primary ice being simply overwhelmed by SIP, it actually determines how SIP affects cloud microphysics.

388   The effect of SIP on the radiative properties of the cloud field is dependent on INP parameterisation choice, both in

389   magnitude and sign of change (Fig. 3b). SIP makes the clouds more reflective independent of the chosen

390   parameterisation (Fig. 3b, cloudy regions contribution) due to increases in snow and cloud droplet water path. N12

391   and A13 have the largest overall radiative response to SIP because changes to the radiative forcing from cloudy

392   regions and cloud fraction contributions act to increase outgoing radiation (Fig. 3b). However, the cloud fraction

393   response to SIP is opposite for C86, M92 and D10 meaning the cloudy regions and cloud fraction contributions act in

394   opposite directions, reducing the total radiative forcing.

395   The different response of the domain cloud fraction to the presence of SIP is caused by substantial variation between

396   simulations in the anvil cloud extent (Fig. 7h), from an increase of 10% (+0.9% of the domain area) in N12 to a

397   decrease of 40% (-3.6% of the domain area) in M92 (Fig. 7h). These non-uniform changes in cloud fraction and

398   outgoing radiation can be explained by differences in the response of cloud freezing profiles to SIP due to variations in

399   INP parameterisation slope. For all INP parameterisations, SIP reduces the availability of liquid at higher altitudes. For

400   shallower parameterisations such as M92 this causes a reduction in the amount of cloud droplets reaching the

401   homogeneous freezing regime and thereby reduces ICNC and cloud anvil spatial extent. However, in simulations using

402   a steep parameterisation, almost all available droplets are frozen heterogeneously before they reach the

403   homogeneous regime (see reduced homogeneous ice production rates in N12 and A13 in Fig. A5b). Therefore, in

404   simulations using a steeper parameterisation, such as N12, a reduction in liquid availability due to SIP occurs at the

405   top of the heterogeneous freezing regime, reducing the availability of liquid for riming, causing a reduction in frozen

406   hydrometeor size at high altitudes, a reduction in hydrometeor sedimentation and an increase in anvil extent. Overall,

407   our simulations show that INP parameterisation choice and slope is an important determinant of cloud field micro-

408   and macrophysical properties, even when SIP is active, and that choice of INP parameterisation affects the cloud field

409   response to SIP.

410

4. Limitations of this modelling study

411

412   The lack of consideration of ice and snow particle number by the SOCRATES radiation scheme is an important

413   limitation of the results presented here. Changes to ICNC, without a co-occurring change in ice crystal mass

414   concentrations, will not be reflected in modelled radiative fluxes. However, our results are still very relevant for

415   climate model simulations as climate models do not typically represent ICNCs and have frequently been shown to

416   poorly represent ice crystal mass concentrations (Baran et al., 2014; Waliser et al., 2009). The SOCRATES

417   representation of radiation with a dependence on ice mass is a more accurate and realistic representation of radiation

418   than is seen in many climate models which often derive bulk optical properties using empirically derived deterministic

419   relationships between ice particle size and environmental temperature and/or ice water content (Baran et al., 2014;

420   Edwards et al., 2007; Fu et al., 1999; Gu et al., 2011). However, the effect of INP parameterisation on deep convective

421   clouds radiative properties using a radiation code that considers ice particle number should be explored in future

422   studies. The sensitivity of the cloud field to the chosen INP parameterisation and SIP indicates the importance of

423   accurately representing ice water content in climate models and linking this ice water content to ice-nucleating

424   particle type.

425   Another limitation of the SOCRATES radiation code is its lack of consideration of rain and graupel particles. The effects

426   of these hydrometeors are expected to be less than that of ice, snow and cloud droplets as they precipitate faster and

427   therefore have a shorter lifetime. Furthermore, the effect of graupel on the tropical longwave radiative effect has

428   been found to be negligible and dwarfed by that of snow (Chen et al., 2018). The global radiative effect of rain has also

429   been found to be small in the vast majority of cases even at high temporal and spatial resolution (Hill et al., 2018). The

430   effect of the incorporation of these hydrometeors into radiative transfer parameterisations should however be tested

431   in future studies.

432   The use of both aerosol-dependent (D10, N12, A13) and solely-temperature dependent (C86, M92) parameterisations

433   in this study means that we have examined the radiative sensitivity of a complex cloud field to a larger variety of INP

434   parameterisations used in weather and climate models than if we had exclusively used parameterisations that

435   consider aerosol concentration. However, this experimental design has limitations. For example, due to the lack of

436   aerosol dependence of the C86 and M92 schemes a 'presumed' dust concentration is implicitly present in these two

437   cases and remains uniform throughout the simulation period. The effect of INP parameterisation choice on convective

438   cloud field properties should also be examined with the inclusion of aerosol scavenging but this was beyond the scope

439   of this study.

440   This study utilised our best estimate of ice production by the Hallett Mossop process (Connolly et al., 2006; Hallett and

441   Mossop, 1974; Mossop, 1985), the most well-studied SIP mechanism, to try and understand the effect of the process,

442   as currently understood, on deep convective cloud properties. However, this rate of ice production is very uncertain

443 and other mechanisms of SIP have also been proposed (Field et al., 2017). Future work will attempt to overcome the

444 above caveats by using statistical emulation (Johnson et al., 2015b) to examine the interacting effects of dust number

445 concentration, INP parameterisation slope and SIP in an idealised deep convective cloud.

446

447 5. Conclusions

448 We quantified the effect of INP parameterisation choice on the radiative properties of a deep convective cloud field

449 using a regional model with advanced double-moment capabilities. The simulated domain exceeds 600,000 km^2 and

450 therefore captures the effects of INP and INP parameterisation on a typical large, complex and heterogeneous

451 convective cloud field. The presence of INP increases domain-mean daylight TOA outgoing radiation by between 2.6

452 and 20.8 W m^{-2} and the choice of INP parameterisation can have as large an effect on cloud field properties as the

453 inclusion or exclusion of INP. These effects are evident even in the presence of SIP, refuting the hypothesis that INP is

454 irrelevant beyond a minimum concentration needed to initiate SIP (Crawford et al., 2012; Ladino et al., 2017; Lawson

455 et al., 2015; Phillips et al., 2007). Furthermore, the effects of SIP on the cloud field properties are strongly dependent

456 on INP parameterisation choice. Both the magnitude and direction of change in cloud fraction and total outgoing

457 radiation due to SIP varies according to INP parameterisation choice. Microphysical alterations to cloud properties are

458 important contributors to radiative differences between simulations, in agreement with previous studies documenting

459 the effect of aerosol-cloud interactions to the radiative forcing by deep convective clouds (Fan et al., 2013). For

460 example, increasing cloud condensation nuclei concentrations, with no perturbations to INP, was shown to increase

461 cloud albedo and cloud fraction, deepen clouds and increase TOA outgoing radiation by 2-4 W m^{-2} (Fan et al., 2013).

462 Here we find that even for the same aerosol and CCN concentrations, just altering the relationship between aerosol

463 concentration and ice-nucleating ability can cause changes in daylight TOA outgoing radiation of up to 18.2 W m^{-2} in

464 our domain.

465 Our results indicate that the slope of the INP parameterisation with respect to temperature (dlog[INP]/dT) is

466 particularly important: Outgoing total radiation, along with many cloud field and microphysical properties affecting

467 radiation, were significantly correlated with INP parameterisation slope. Best practise for accurately representing INP

468 number concentrations based on current knowledge is to utilise parameterisations that link aerosol number and

469 particle size to INP number concentration (e.g. D10, N12, A13) but that is not enough without also using a

470   parameterisation in which the temperature dependence of the INP number concentrations matches reality; the

471   largest differences in domain outgoing radiation existed in this study between simulations using aerosol dependent

472   parameterisations (D10 and A13). These large variations in outgoing radiation between simulations using different

473   aerosol dependent INP parameterisations justifies investment in observational campaigns to more effectively

474   constrain the range of expected INP concentrations and parameterisation slopes in the Saharan dust outflow region,

475   and other regions dominated by maritime deep convective activity.

476   The significance of the slope of the INP parameterisation indicates the potential importance of accounting for

477   differences in aerosol composition in modelling studies. For example, INP derived from marine organics (Wilson et al.,

478   2015) have a shallower slope than mineral dust INP (Atkinson et al., 2013; Niemand et al., 2012). Furthermore, real-

479   world INP concentrations are known to have complex temperature dependencies with biological INP, such as soil

480   borne fungus and plant related bacteria, making significant contributions at the warmest temperatures and mineral

481   components being more important at lower temperatures (O'Sullivan et al., 2018). The work here suggests that the

482   presence of biological INP might be to reduce liquid water transport to the upper levels of the cloud, reducing cirrus

483   anvil extent, but also to increase low cloud fraction. Nevertheless, measurements in the eastern tropical Atlantic

484   indicate that biological INP in the Saharan dust plumes is at most a minor contribution and that the parameterisations

485   with shallow slope in Fig. 1 produce too much glaciation at warm temperatures.

486   The results presented here also present a new framework for understanding the effect of SIP by identifying a potential

487   relationship between the effect of the Hallett Mossop process and INP parameterisation slope. The significance of INP

488   parameterisation slope also highlights the importance of characterising the INP concentration across the entirety of

489   the mixed-phase temperature range rather than just at one temperature, or in a narrow temperature range, as is

490   common in many field campaigns. For example, in the ICE-D field campaign, INP concentrations at temperatures

491   above -7 and below -27°C were not measurable due to experimental and sampling constraints (Price et al., 2018).

492   Measuring INP over the entire mixed-phase temperature range, throughout which deep convective clouds extend,

493   conceivably covering around 10 orders of magnitude in INP number concentration, represents a major experimental

494   challenge. This issue is compounded by the fact that INP spectra cannot reliably be extrapolated to higher or lower

495   temperatures since our underpinning physical understanding of what makes an effective nucleation site is lacking

496   (Holden et al., 2019). This work demonstrates the importance of solving these problems and measuring INP number

497   concentrations across the entirety of the mixed-phase temperature spectrum.

Data Availability

The datasets generated and analysed in this study are available from the corresponding author on reasonable request.

Author Contributions

REH, AKM, KSC, PRF and BJM contributed to the design, development and direction of the study. REH and AKM set up

and ran the UM-CASIM simulations presented in the paper. REH processed and analysed the UM-CASIM datasets.

JMW, AAH and BJS built and maintained the Met-Office CASIM model used to run the simulations. ZC and RJC

provided processed aircraft data from the ICE-D b933 flight and helped with the comparison of model data with

aircraft measurements. REH, AKM, JMW, AAH, ZC, RJC, KSC, PRF and BJM edited the manuscript.

Competing interests

The authors declare no competing interests.

Acknowledgements

This work has been funded by European Research Council (ERC, grant 648661 MarineIce) and the Natural Environment

Research Council (NERC, grant NE/M00340X/1). We acknowledge the use of Monsoon, a collaborative High

Performance Computing facility funded by the Met Office and NERC. We acknowledge the use of JASMIN, the UK

collaborative data analysis facility. We obtained moderate resolution imaging spectroradiometer (MODIS) Corrected

Reflectance images from the NASA Worldview website (https://worldview.earthdata.nasa.gov/). Airborne

measurements were obtained from the ICE-D field campaign and specifically the b933 flight on the 21st August 2015.

The ICE-D campaign used the BAe-146-301 Atmospheric Research Aircraft which is operated by Directflight Ltd (now

Airtask) and managed by the Facility for Airborne Atmospheric Measurements (FAAM). At the time of the

measurements FAAM was a joint entity of NERC and the UK Met Office. We thank all the people involved in the ICE-D

campaign.

520 ## **References**

521 Abdul-Razzak, H. and Ghan, S. J.: A parameterization of aerosol activation: 2. Multiple aerosol types, J. Geophys. Res.,

522 105(16), 6837–6844, doi:10.1029/1999JD901161, 2000.

523 Arakawa, A.: The cumulus parameterization problem: Past, present, and future, J. Clim., 17(13), 2493–2525,

524 doi:10.1175/1520-0442(2004)017<2493:RATCPP>2.0.CO;2, 2004.

525 Atkinson, J. D., Murray, B. J., Woodhouse, M. T., Whale, T. F., Baustian, K. J., Carslaw, K. S., Dobbie, S., O'Sullivan, D.

526 and Malkin, T. L.: The importance of feldspar for ice nucleation by mineral dust in mixed-phase clouds, Nature,

527 498(7454), 355–358, doi:10.1038/nature12278, 2013.

528 Baran, A. J., Hill, P., Furtado, K., Field, P. and Manners, J.: A Coupled Cloud Physics–Radiation Parameterization of the

529 Bulk Optical Properties of Cirrus and Its Impact on the Met Office Unified Model Global Atmosphere 5.0 Configuration,

530 J. Clim., 27(20), 7725–7752, doi:10.1175/JCLI-D-13-00700.1, 2014.

531 Bigg, E. K.: The formation of atmospheric ice crystals by the freezing of droplets, Q. J. R. Meteorol. Soc., 79(342), 510–

532 519, doi:10.1002/qj.49707934207, 1953.

533 Boose, Y., Kanji, Z. A., Kohn, M., Sierau, B., Zipori, A., Crawford, I., Lloyd, G., Bukowiecki, N., Herrmann, E., Kupiszewski,

534 P., Steinbacher, M. and Lohmann, U.: Ice nucleating particle measurements at 241K during winter months at 3580m

535 MSL in the swiss alps, J. Atmos. Sci., 73(5), 2203–2228, doi:10.1175/JAS-D-15-0236.1, 2016a.

536 Boose, Y., Sierau, B., García, M. I., Rodríguez, S., Alastuey, A., Linke, C., Schnaiter, M., Kupiszewski, P., Kanji, Z. A. and

537 Lohmann, U.: Ice nucleating particles in the Saharan Air Layer, Atmos. Chem. Phys., 16(14), 9067–9087,

538 doi:10.5194/acp-16-9067-2016, 2016b.

539 Cantrell, W. and Heymsfield, A.: Production of ice in tropospheric clouds: a review, Bull. Am. Meteorol. Soc., 86(6),

540 795–808, doi:10.1175/BAMS-86-6-795, 2005.

541 Carrió, G. G., van den Heever, S. C. and Cotton, W. R.: Impacts of nucleating aerosol on anvil-cirrus clouds: A modeling

542 study, Atmos. Res., 84(2), 111–131, doi:10.1016/j.atmosres.2006.06.002, 2007.

543 Chen, Y., Seiki, T., Kodama, C., Satoh, M. and Noda, A. T.: Impact of Precipitating Ice Hydrometeors on Longwave

544 Radiative Effect Estimated by a Global Cloud-System Resolving Model, J. Adv. Model. Earth Syst., 10(2), 284–296,

545 doi:10.1002/2017MS001180, 2018.

546 Connolly, P. J., Choularton, T. W., Gallagher, M. W., Bower, K. N., Flynn, M. J. and Whiteway, J. A.: Cloud-resolving

547 simulations of intense tropical Hector thunderstorms: Implications for aerosol-cloud interactions, Meteorol. Soc, 132,

548 3079–3106, doi:10.1256/qj.05.86, 2006.

549 Cooper, W. A.: Ice initiation in natural clouds, in Precipitation enhancement—A scientific challenge, pp. 29–32,

550 American Meteorological Society, Boston, MA., 1986.

551 Crawford, I., Bower, K. N., Choularton, T. W., Dearden, C., Crosier, J., Westbrook, C., Capes, G., Coe, H., Connolly, P. J.,

552 Dorsey, J. R., Gallagher, M. W., Williams, P., Trembath, J., Cui, Z. and Blyth, A.: Ice formation and development in aged,

553 wintertime cumulus over the UK: observations and modelling, Atmos. Chem. Phys., 12(11), 4963–4985,

554 doi:10.5194/acp-12-4963-2012, 2012.

555   DeMott, P. J., Sassen, K., Poellot, M. R., Baumgardner, D., Rogers, D. C., Brooks, S. D., Prenni, A. J. and Kreidenweis, S.

556   M.: African dust aerosols as atmospheric ice nuclei, Geophys. Res. Lett., 30(14), 1732–1726,

557   doi:10.1029/2003GL017410, 2003.

558   DeMott, P. J., Prenni, A. J., Liu, X., Kreidenweis, S. M., Petters, M. D., Twohy, C. H., Richardson, M. S., Eidhammer, T.

559   and Rogers, D. C.: Predicting global atmospheric ice nuclei distributions and their impacts on climate., Proc. Natl. Acad.

560   Sci. U. S. A., 107(25), 11217–22, doi:10.1073/pnas.0910818107, 2010.

561   DeMott, P. J., Prenni, A. J., McMeeking, G. R., Sullivan, R. C., Petters, M. D., Tobo, Y., Niemand, M., Möhler, O., Snider,

562   J. R., Wang, Z. and Kreidenweis, S. M.: Integrating laboratory and field data to quantify the immersion freezing ice

563   nucleation activity of mineral dust particles, Atmos. Chem. Phys, 15, 393–409, doi:10.5194/acp-15-393-2015, 2015.

564   Deng, X., Xue, H. and Meng, Z.: The effect of ice nuclei on a deep convective cloud in South China, Atmos. Res., 206, 1–

565   12, doi:10.1016/J.ATMOSRES.2018.02.013, 2018.

566   Edwards, J. M. and Slingo, A.: Studies with a flexible new radiation code. I: Choosing a configuration for a large-scale

567   model, Q. J. R. Meteorol. Soc., 122(531), 689–719, doi:10.1002/qj.49712253107, 1996.

568   Edwards, J. M., Havemann, S., Thelen, J. C. and Baran, A. J.: A new parametrization for the radiative properties of ice

569   crystals: Comparison with existing schemes and impact in a GCM, Atmos. Res., 83(1), 19–35,

570   doi:10.1016/j.atmosres.2006.03.002, 2007.

571   Eidhammer, T., Demott, P. J. and Kreidenweis, S. M.: A comparison of heterogeneous ice nucleation parameterizations

572   using a parcel model framework, J. Geophys. Res. Atmos., 114(6), doi:10.1029/2008JD011095, 2009.

573   Ekman, A. M. L., Engström, A. and Wang, C.: The effect of aerosol composition and concentration on the development

574   and anvil properties of a continental deep convective cloud, Q. J. R. Meteorol. Soc., 133(627), 1439–1452,

575   doi:10.1002/qj.108, 2007.

576   Fan, J., Comstock, J. M. and Ovchinnikov, M.: The cloud condensation nuclei and ice nuclei effects on tropical anvil

577   characteristics and water vapor of the tropical tropopause layer, Environ. Res. Lett., 5(4), 044005, doi:10.1088/1748-

578   9326/5/4/044005, 2010a.

579   Fan, J., Comstock, J. M., Ovchinnikov, M., McFarlane, S. A., McFarquhar, G. and Allen, G.: Tropical anvil characteristics

580   and water vapor of the tropical tropopause layer: Impact of heterogeneous and homogeneous freezing

581   parameterizations, J. Geophys. Res., 115(D12), D12201, doi:10.1029/2009JD012696, 2010b.

582   Fan, J., Rosenfeld, D., Ding, Y., Leung, L. R. and Li, Z.: Potential aerosol indirect effects on atmospheric circulation and

583   radiative forcing through deep convection, Geophys. Res. Lett., 39(9), L09806, doi:10.1029/2012GL051851, 2012.

584   Fan, J., Leung, L. R., Rosenfeld, D., Chen, Q., Li, Z., Zhang, J. and Yan, H.: Microphysical effects determine

585   macrophysical response for aerosol impacts on deep convective clouds., Proc. Natl. Acad. Sci. U. S. A., 110(48), E4581-

586   90, doi:10.1073/pnas.1316830110, 2013.

587   Field, P. R., Lawson, R. P., Brown, P. R. A., Lloyd, G., Westbrook, C., Moisseev, D., Miltenberger, A., Nenes, A., Blyth, A.,

588   Choularton, T., Connolly, P., Buehl, J., Crosier, J., Cui, Z., Dearden, C., DeMott, P., Flossmann, A., Heymsfield, A., Huang,

589   Y., Kalesse, H., Kanji, Z. A., Korolev, A., Kirchgaessner, A., Lasher-Trapp, S., Leisner, T., McFarquhar, G., Phillips, V.,

590   Stith, J., Sullivan, S., Field, P. R., Lawson, R. P., Brown, P. R. A., Lloyd, G., Westbrook, C., Moisseev, D., Miltenberger, A.,

591   Nenes, A., Blyth, A., Choularton, T., Connolly, P., Buehl, J., Crosier, J., Cui, Z., Dearden, C., DeMott, P., Flossmann, A.,

592   Heymsfield, A., Huang, Y., Kalesse, H., Kanji, Z. A., Korolev, A., Kirchgaessner, A., Lasher-Trapp, S., Leisner, T.,

593   McFarquhar, G., Phillips, V., Stith, J. and Sullivan, S.: Chapter 7. Secondary ice production - current state of the science

594   and recommendations for the future, Meteorol. Monogr., 7.1-7.20 [online] Available from:

595   http://journals.ametsoc.org/doi/10.1175/AMSMONOGRAPHS-D-16-0014.1 (Accessed 4 April 2017), 2017.

596   Fridlind, A. M., Ackerman, A. S., McFarquhar, G., Zhang, G., Poellot, M. R., DeMott, P. J., Prenni, A. J. and Heymsfield,

597   A. J.: Ice properties of single-layer stratocumulus during the Mixed-Phase Arctic Cloud Experiment: 2. Model results, J.

598   Geophys. Res., 112(D24), D24202, doi:10.1029/2007JD008646, 2007.

599   Fu, Q., Sun, W. B., Yang, P., Fu, Q., Sun, W. B. and Yang, P.: Modeling of Scattering and Absorption by Nonspherical

600   Cirrus Ice Particles at Thermal Infrared Wavelengths, http://dx.doi.org/10.1175/1520-

601   0469(1999)056<2937:MOSAAB>2.0.CO;2, doi:10.1175/1520-0469(1999)056<2937:MOSAAB>2.0.CO;2, 1999.

602   Gibbons, M., Min, Q. and Fan, J.: Investigating the impacts of Saharan dust on tropical deep convection using spectral

603   bin microphysics, Atmos. Chem. Phys, 18, 12161–12184, doi:10.5194/acp-18-12161-2018, 2018.

604   Grosvenor, D. P., Field, P. R., Hill, A. A. and Shipway, B. J.: The relative importance of macrophysical and cloud albedo

605   changes for aerosol-induced radiative effects in closed-cell stratocumulus: insight from the modelling of a case study,

606   Atmos. Chem. Phys, 17, 5155–5183, doi:10.5194/acp-17-5155-2017, 2017.

607   Gu, Y., Liou, K. N., Ou, S. C. and Fovell, R.: Cirrus cloud simulations using WRF with improved radiation

608   parameterization and increased vertical resolution, J. Geophys. Res., 116(D6), D06119, doi:10.1029/2010JD014574,

609   2011.

610   Hallett, J. and Mossop, S. C.: Production of secondary ice particles during the riming process, Nature, 249(5452), 26–

611   28, doi:10.1038/249026a0, 1974.

612   Harrison, A. D., Whale, T. F., Carpenter, M. A., Holden, M. A., Neve, L., O'Sullivan, D., Vergara Temprado, J. and

613   Murray, B. J.: Not all feldspars are equal: a survey of ice nucleating properties across the feldspar group of minerals,

614   Atmos. Chem. Phys., 16(17), 10927–10940, doi:10.5194/acp-16-10927-2016, 2016.

615   Harrison, A. D., Lever, K., Sanchez-Marroquin, A., Holden, M. A., Whale, T. F., Tarn, M. D., McQuaid, J. B. and Murray,

616   B. J.: The ice-nucleating ability of quartz immersed in water and its atmospheric importance compared to K-feldspar,

617   Atmos. Chem. Phys., 19(17), 11343–11361, doi:10.5194/acp-19-11343-2019, 2019.

618   van den Heever, S. C., Carrió, G. G., Cotton, W. R., DeMott, P. J. and Prenni, A. J.: Impacts of nucleating aerosol on

619   Florida storms. Part I: Mesoscale simulations, J. Atmos. Sci., 63(7), 1752–1775, doi:10.1175/JAS3713.1, 2006.

620   Herbert, R. J., Murray, B. J., Dobbie, S. J. and Koop, T.: Sensitivity of liquid clouds to homogenous freezing

621   parameterizations, Geophys. Res. Lett., 42(5), 1599–1605, doi:10.1002/2014GL062729@10.1002/(ISSN)1944-

622   8007.2015EDHIGHLIGHTS, 2015.

623   Heymsfield, A. and Willis, P.: Cloud conditions favoring secondary ice particle production in tropical maritime

624   convection, J. Atmos. Sci., 71(12), 4500–4526, doi:10.1175/JAS-D-14-0093.1, 2014.

625   Heymsfield, A. J. and Mossop, S. C.: Temperature dependence of secondary ice crystal production during soft hail

626   growth by riming, Q. J. R. Meteorol. Soc., 110(465), 765–770, doi:10.1002/qj.49711046512, 1984.

627   Hill, P. G., Chiu, J. C., Allan, R. P. and Chern, J. -D.: Characterizing the Radiative Effect of Rain Using a Global Ensemble

628   of Cloud Resolving Simulations, J. Adv. Model. Earth Syst., 10(10), 2453–2470, doi:10.1029/2018MS001415, 2018.

629   Holden, M. A., Whale, T. F., Tarn, M. D., O'Sullivan, D., Walshaw, R. D., Murray, B. J., Meldrum, F. C. and Christenson,

630   H. K.: High-speed imaging of ice nucleation in water proves the existence of active sites, Sci. Adv., 5(2),

631   doi:10.1126/sciadv.aav4316, 2019.

632   Huang, Y., Blyth, A. M., Brown, P. R. A., Choularton, T. W. and Cui, Z.: Factors controlling secondary ice production in

633   cumulus clouds, Q. J. R. Meteorol. Soc., 143(703), 1021–1031, doi:10.1002/qj.2987, 2017.

634   Jeffery, C. A. and Austin, P. H.: Homogeneous nucleation of supercooled water: Results from a new equation of state,

635   J. Geophys. Res. Atmos., 102(21), 25269–25279, doi:10.1029/97jd02243, 1997.

636   Johnson, C. E., Bellouin, N., Davison, P. S., Jones, A., Rae, J. G. L., Roberts, D. L., Woodage, M. J., Woodward, S., Or Õ

637   Nez, C. and Savage, N. H.: CLASSIC Aerosol Scheme, Unified Model Doc. Pap. (Vn 10.3) [online] Available from:

638   https://code.metoffice.gov.uk/doc/um/vn10.3/papers/umdp_020.pdf (Accessed 9 March 2017a), 2015.

639   Johnson, J. S., Cui, Z., Lee, L. A., Gosling, J. P., Blyth, A. M. and Carslaw, K. S.: Evaluating uncertainty in convective cloud

640   microphysics using statistical emulation, J. Adv. Model. Earth Syst., 7(1), 162–187, doi:10.1002/2014MS000383,

641   2015b.

642   Kanji, Z. A., Ladino, L. A., Wex, H., Boose, Y., Burkert-Kohn, M., Cziczo, D. J., Krämer, M., Kanji, Z. A., Ladino, L. A., Wex,

643   H., Boose, Y., Burkert-Kohn, M., Cziczo, D. J. and Krämer, M.: Overview of Ice Nucleating Particles, Meteorol. Monogr.,

644   58, 1.1-1.33, doi:10.1175/AMSMONOGRAPHS-D-16-0006.1, 2017.

645   Lacher, L., Steinbacher, M., Bukowiecki, N., Herrmann, E., Zipori, A. and Kanji, Z. A.: Impact of air mass conditions and

646   aerosol properties on ice nucleating particle concentrations at the High Altitude Research Station Jungfraujoch,

647   Atmosphere (Basel)., 9(9), 363, doi:10.3390/atmos9090363, 2018.

648   Ladino, L. A., Korolev, A., Heckman, I., Wolde, M., Fridlind, A. M. and Ackerman, A. S.: On the role of ice-nucleating

649   aerosol in the formation of ice particles in tropical mesoscale convective systems, Geophys. Res. Lett., 44(3), 1574–

650   1582, doi:10.1002/2016GL072455, 2017.

651   Lasher-Trapp, S., Leon, D. C., DeMott, P. J., Villanueva-Birriel, C. M., Johnson, A. V., Moser, D. H., Tully, C. S. and Wu,

652   W.: A Multisensor Investigation of Rime Splintering in Tropical Maritime Cumuli, J. Atmos. Sci., 73(6), 2547–2564,

653   doi:10.1175/JAS-D-15-0285.1, 2016.

654   Lawson, R. P., Woods, S., Morrison, H., Lawson, R. P., Woods, S. and Morrison, H.: The Microphysics of Ice and

655   Precipitation Development in Tropical Cumulus Clouds, J. Atmos. Sci., 72(6), 2429–2445, doi:10.1175/JAS-D-14-0274.1,

656   2015.

657   Liu, X., Fu, Y., Cao, Z. and Jin, S.: Influence of ice nuclei parameterization schemes on the hail process, Adv. Meteorol.,

658   2018, doi:10.1155/2018/4204137, 2018.

659   Lloyd, G., Choularton, T., Bower, K., Crosier, J., Gallagher, M., Flynn, M., Dorsey, J., Liu, D., Taylor, J. W., Schlenczek, O.,

660   Fugal, J., Borrmann, S., Cotton, R., Field, P. and Blyth, A.: Small Ice Particles at Slightly Supercooled Temperatures in

661   Tropical Maritime Convection, Atmos. Chem. Phys. Discuss., 1–18, doi:10.5194/acp-2019-345, 2019.

662 Lohmann, U., Lüönd, F. and Mahrt, F.: An introduction to clouds: From the microscale to climate, Cambridge

663 University Press., 2016.

664 Luo, Z. and Rossow, W. B.: Characterizing tropical cirrus life cycle, evolution, and interaction with upper-tropospheric

665 water vapor using lagrangian trajectory analysis of satellite observations, J. Clim., 17(23), 4541–4563,

666 doi:10.1175/3222.1, 2004.

667 Mace, G. G., Deng, M., Soden, B. and Zipser, E.: Association of tropical cirrus in the 10–15-km layer with deep

668 convective sources: An observational study combining millimeter radar sata and satellite-derived trajectories, J.

669 Atmos. Sci., 63(2), 480–503, doi:10.1175/JAS3627.1, 2006.

670 Manners, J., Edwards, J. M., Hill, P. and Thelen, J.-C.: SOCRATES technical guide Suite Of Community RAdiative Transfer

671 codes based on Edwards and Slingo., 2017.

672 McCoy, D. T., Field, P. R., Schmidt, A., Grosvenor, D. P., A-M Bender, F., Shipway, B. J., Hill, A. A., Wilkinson, J. M. and

673 Elsaesser, G. S.: Aerosol midlatitude cyclone indirect effects in observations and high-resolution simulations, Atmos.

674 Chem. Phys, 18, 5821–5846, doi:10.5194/acp-18-5821-2018, 2018.

675 Meyers, M. P., DeMott, P. J., Cotton, W. R., Meyers, M. P., DeMott, P. J. and Cotton, W. R.: New primary ice-nucleation

676 parameterizations in an explicit cloud model, J. Appl. Meteorol., 31(7), 708–721, doi:10.1175/1520-

677 0450(1992)031<0708:NPINPI>2.0.CO;2, 1992.

678 Miltenberger, A. K., Field, P. R., Hill, A. A., Rosenberg, P., Shipway, B. J., Wilkinson, J. M., Scovell, R. and Blyth, A. M.:

679 Aerosol–cloud interactions in mixed-phase convective clouds – Part 1: Aerosol perturbations, Atmos. Chem. Phys.,

680 18(5), 3119–3145, doi:10.5194/acp-18-3119-2018, 2018.

681 Mossop, S. C.: Secondary ice particle production during rime growth: The effect of drop size distribution and rimer

682 velocity, Q. J. R. Meteorol. Soc., 111(470), 1113–1124, doi:10.1002/qj.49711147012, 1985.

683 Niemand, M., Möhler, O., Vogel, B., Vogel, H., Hoose, C., Connolly, P., Klein, H., Bingemer, H., DeMott, P., Skrotzki, J.,

684 Leisner, T., Niemand, M., Möhler, O., Vogel, B., Vogel, H., Hoose, C., Connolly, P., Klein, H., Bingemer, H., DeMott, P.,

685 Skrotzki, J. and Leisner, T.: A particle-surface-area-based parameterization of immersion freezing on desert dust

686 particles, J. Atmos. Sci., 69(10), 3077–3092, doi:10.1175/JAS-D-11-0249.1, 2012.

687 O'Sullivan, D., Adams, M. P., Tarn, M. D., Harrison, A. D., Vergara-Temprado, J., Porter, G. C. E., Holden, M. A.,

688 Sanchez-Marroquin, A., Carotenuto, F., Whale, T. F., McQuaid, J. B., Walshaw, R., Hedges, D. H. P., Burke, I. T., Cui, Z.

689 and Murray, B. J.: Contributions of biogenic material to the atmospheric ice-nucleating particle population in North

690 Western Europe, Sci. Rep., 8(1), doi:10.1038/s41598-018-31981-7, 2018.

691 Phillips, V. T. J., Andronache, C., Sherwood, S. C., Bansemer, A., Conant, W. C., Demott, P. J., Flagan, R. C., Heymsfield,

692 A., Jonsson, H., Poellot, M., Rissman, T. A., Seinfeld, J. H., Vanreken, T., Varutbangkul, V. and Wilson, J. C.: Anvil

693 glaciation in a deep cumulus updraught over Florida simulated with the Explicit Microphysics Model. I: Impact of

694 various nucleation processes, Q. J. R. Meteorol. Soc., 131(609), 2019–2046, doi:10.1256/qj.04.85, 2005.

695 Phillips, V. T. J., Donner, L. J., Garner, S. T., Phillips, V. T. J., Donner, L. J. and Garner, S. T.: Nucleation processes in deep

696 convection simulated by a cloud-system-resolving model with double-moment bulk microphysics, J. Atmos. Sci., 64(3),

697 738–761, doi:10.1175/JAS3869.1, 2007.

698 Phillips, V. T. J., Patade, S., Gutierrez, J. and Bansemer, A.: Secondary Ice Production by Fragmentation of Freezing

699 Drops: Formulation and Theory, J. Atmos. Sci., 75, 3031–3070, doi:10.1175/JAS-D-17-0190.1, 2018.

700 Price, H. C., Baustian, K. J., McQuaid, J. B., Blyth, A., Bower, K. N., Choularton, T., Cotton, R. J., Cui, Z., Field, P. R.,

701 Gallagher, M., Hawker, R., Merrington, A., Miltenberger, A., Neely III, R. R., Parker, S. T., Rosenberg, P. D., Taylor, J. W.,

702 Trembath, J., Vergara-Temprado, J., Whale, T. F., Wilson, T. W., Young, G. and Murray, B. J.: Atmospheric ice-

703 nucleating particles in the dusty tropical Atlantic, J. Geophys. Res. Atmos., 123(4), 2175–2193,

704 doi:10.1002/2017JD027560, 2018.

705 Saunders, C. P. . and Hosseini, A. .: A laboratory study of the effect of velocity on Hallett–Mossop ice crystal

706 multiplication, Atmos. Res., 59–60, 3–14, doi:10.1016/S0169-8095(01)00106-5, 2001.

707 Seinfeld, J. H. and Spyros, N. P.: Atmospheric Chemistry and Physics: From Air Pollution to Climate Change, 3rd ed.,

708 Wiley, New York, USA. [online] Available from: https://www.amazon.co.uk/Atmospheric-Chemistry-Physics-Pollution-

709 Climate/dp/0471720186 (Accessed 29 October 2019), 2006.

710 Stevens, R. G., Loewe, K., Dearden, C., Dimitrelos, A., Possner, A., Eirund, G. K., Raatikainen, T., Hill, A. A., Shipway, B.

711 J., Wilkinson, J., Romakkaniemi, S., Tonttila, J., Laaksonen, A., Korhonen, H., Connolly, P., Lohmann, U., Hoose, C.,

712 Ekman, A. M. L., Carslaw, K. S. and Field, P. R.: A model intercomparison of CCN-limited tenuous clouds in the high

713 Arctic, Atmos. Chem. Phys, 18, 11041–11071, doi:10.5194/acp-18-11041-2018, 2018.

714 Sullivan, S. C., Hoose, C., Kiselev, A., Leisner, T. and Nenes, A.: Initiation of secondary ice production in clouds, Atmos.

715 Chem. Phys, 18, 1593–1610, doi:10.5194/acp-18-1593-2018, 2018.

716 Takeishi, A. and Storelvmo, T.: A study of enhanced heterogeneous ice nucleation in simulated deep convective clouds

717 observed during DC3, J. Geophys. Res. Atmos., 123(23), 13,396-13,420, doi:10.1029/2018JD028889, 2018.

718 Vali, G., Demott, P. J., Möhler, O. and Whale, T. F.: Technical Note: A proposal for ice nucleation terminology, Atmos.

719 Chem. Phys, 15, 10263–10270, doi:10.5194/acp-15-10263-2015, 2015.

720 Vergara-Temprado, J., Murray, B. J., Wilson, T. W., O'sullivan, D., Browse, J., Pringle, K. J., Ardon-Dryer, K., Bertram, A.

721 K., Burrows, S. M., Ceburnis, D., Demott, P. J., Mason, R. H., O'dowd, C. D., Rinaldi, M. and Carslaw, K. S.: Contribution

722 of feldspar and marine organic aerosols to global ice nucleating particle concentrations, Atmos. Chem. Phys, 17, 3637–

723 3658, doi:10.5194/acp-17-3637-2017, 2017.

724 Vergara-Temprado, J., Miltenberger, A. K., Furtado, K., Grosvenor, D. P., Shipway, B. J., Hill, A. A., Wilkinson, J. M.,

725 Field, P. R., Murray, B. J. and Carslaw, K. S.: Strong control of Southern Ocean cloud reflectivity by ice-nucleating

726 particles., Proc. Natl. Acad. Sci. U. S. A., 115(11), 2687–2692, doi:10.1073/pnas.1721627115, 2018.

727 Waliser, D. E., Li, J. L. F., Woods, C. P., Austin, R. T., Bacmeister, J., Chern, J., Del Genio, A., Jiang, J. H., Kuang, Z., Meng,

728 H., Minnis, P., Platnick, S., Rossow, W. B., Stephens, G. L., Sun-Mack, S., Tao, W. K., Tompkins, A. M., Vane, D. G.,

729 Walker, C. and Wu, D.: Cloud ice: A climate model challenge with signs and expectations of progress, J. Geophys. Res.

730 Atmos., 114(8), doi:10.1029/2008JD010015, 2009.

731 Walters, D., Boutle, I., Brooks, M., Melvin, T., Stratton, R., Vosper, S., Wells, H., Williams, K., Wood, N., Allen, T.,

732 Bushell, A., Copsey, D., Earnshaw, P., Edwards, J., Gross, M., Hardiman, S., Harris, C., Heming, J., Klingaman, N., Levine,

733 R., Manners, J., Martin, G., Milton, S., Mittermaier, M., Morcrette, C., Riddick, T., Roberts, M., Sanchez, C., Selwood, P.,

734   Stirling, A., Smith, C., Suri, D., Tennant, W., Luigi Vidale, P., Wilkinson, J., Willett, M., Woolnough, S. and Xavier, P.: The

735   Met Office Unified Model Global Atmosphere 6.0/6.1 and JULES Global Land 6.0/6.1 configurations, Geosci. Model

736   Dev., 10(4), 1487–1520, doi:10.5194/gmd-10-1487-2017, 2017.

737   Welti, A., Müller, K., Fleming, Z. L. and Stratmann, F.: Concentration and variability of ice nuclei in the subtropical

738   maritime boundary layer, Atmos. Chem. Phys, 18, 5307–5320, doi:10.5194/acp-18-5307-2018, 2018.

739   Wilson, T. W., Ladino, L. A., Alpert, P. A., Breckels, M. N., Brooks, I. M., Browse, J., Burrows, S. M., Carslaw, K. S.,

740   Huffman, J. A., Judd, C., Kilthau, W. P., Mason, R. H., McFiggans, G., Miller, L. A., Nájera, J. J., Polishchuk, E., Rae, S.,

741   Schiller, C. L., Si, M., Temprado, J. V., Whale, T. F., Wong, J. P. S., Wurl, O., Yakobi-Hancock, J. D., Abbatt, J. P. D., Aller,

742   J. Y., Bertram, A. K., Knopf, D. A. and Murray, B. J.: A marine biogenic source of atmospheric ice-nucleating particles,

743   Nature, 525(7568), 234–238, doi:10.1038/nature14986, 2015.

744

745

746 **Figures**
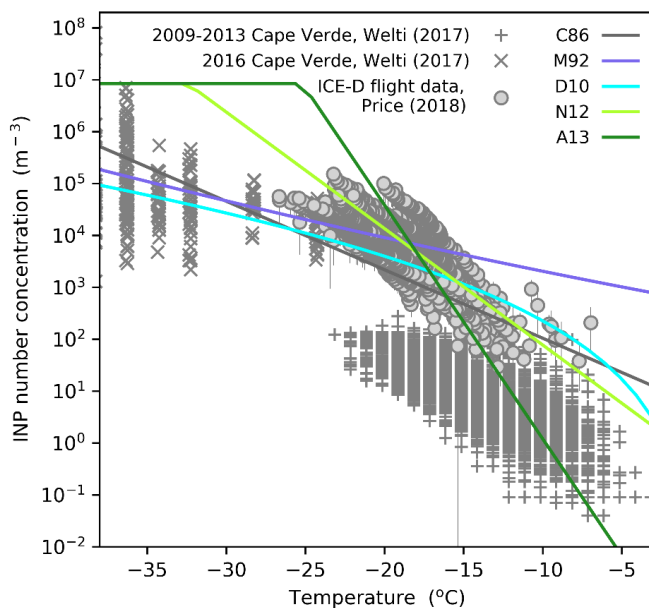
747

748 Figure 1. Dependence of INP number concentration on temperature ($d[INP]/dT$) for the five heterogeneous freezing

749 parameterisations simulated in this study (C86, M92, D10, N12, A13) compared to INP number concentrations measured

750 in the eastern Tropical Atlantic(Price et al., 2018; Welti et al., 2018). Parameterisations are shown for the aerosol

751 concentrations at approximately the first freezing level in our simulations (~ 8 cm^{-3}). D10, N12 and A13 are dependent on

752 aerosol concentrations, while C86 and M92 are not dependent on aerosol concentration. For the correlation analysis

753 where model outputs were plotted against parameterisation slope (dlog$_{10}$[INP]/dT), a straight line was fitted to the

754 D10 parameterisation between -3 and -37°C to obtain an approximate INP parameterisation slope. Other

755 temperature ranges were tested and were found to have no notable effect on results.

756

757
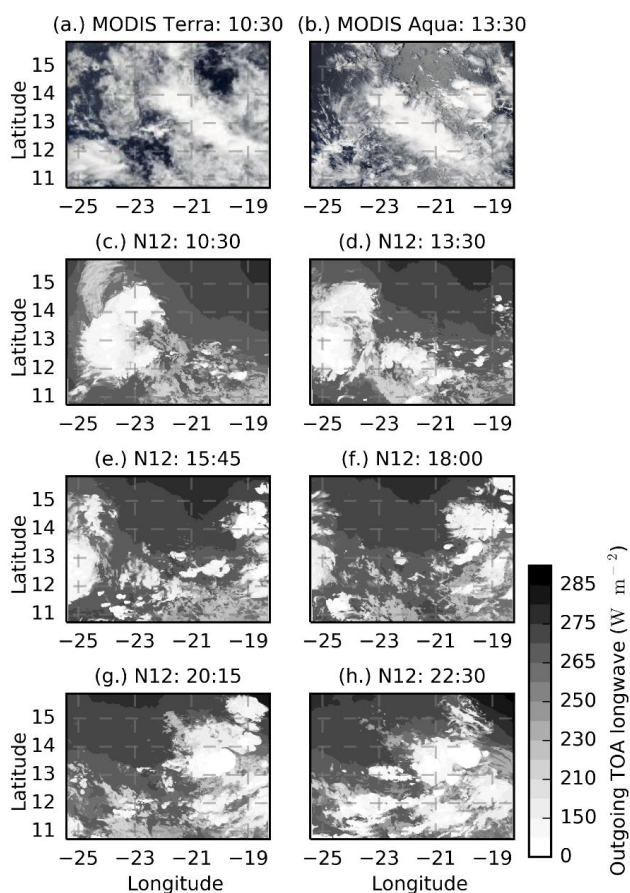
Figure 2. Cloud field evolution. MODIS Terra (a) and Aqua (b) corrected reflectance images of the modelled domain for the 21st of August 2015 and the simulated top of atmosphere outgoing longwave radiation for the N12 simulation throughout the study period (c-h).Note that the colour bar relates to panels c-h only. Images shown in (a) and (b) are moderate resolution imaging spectroradiometer (MODIS) Corrected Reflectance imagery produced using the MODIS Level 1B data and downloaded from the NASA Worldview website.

763

764
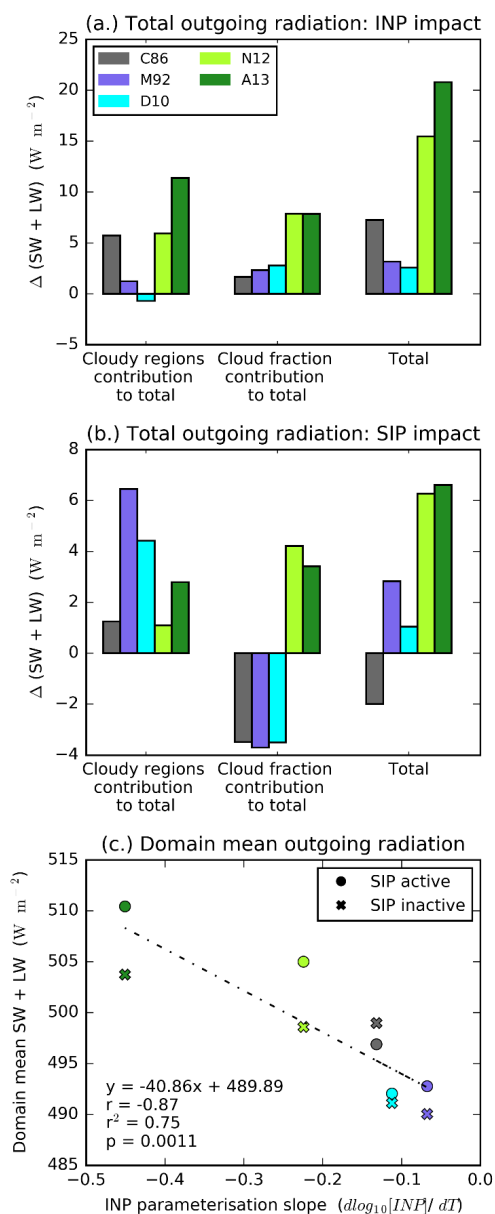
Figure 3. Effect of INP and secondary production on top of atmosphere (TOA) outgoing radiation. Effect of INP

parameterisation (a) and SIP (a representation of the Hallett Mossop process) (b) on domain-mean daytime TOA outgoing

radiation and total domain-mean daytime TOA outgoing radiation plotted against INP parameterisation slope (c). In (a),

the change from the NoINP simulation is shown (INP - NoINP) with SIP active. In (b), the change from SIP_active to

SIP_inactive is shown (SIP_active – SIP_inactive). A positive value indicates more outgoing radiation when INP or SIP are

active. In (a) and (b), the relative contributions of changes in outgoing radiation from cloudy regions (left) and cloud

fraction (middle) to the total radiative forcing (right) are shown (calculation described in Sect. 2.1.3). In addition to the

simulated values, a regression line (n=10) is shown in (c) along with its associated statistical descriptors.
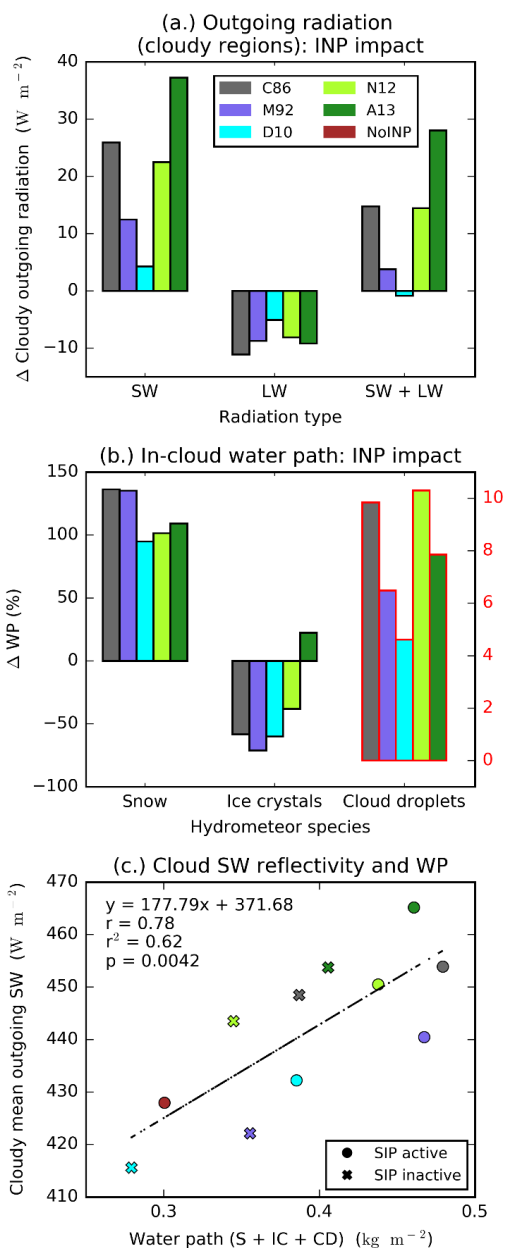
Figure 4. INP and outgoing radiation from cloudy regions. Absolute change in outgoing shortwave, longwave and total radiation from cloudy regions relative to the NoINP simulation (a), the percentage change in water path (WP) associated with snow (S), ice crystals (IC) and cloud droplets (CD) relative to the NoINP simulation (b), and mean daytime outgoing shortwave from cloudy regions plotted against the sum of S, IC and CD water paths (c). Note different scale for CD water path in (b). In addition to the simulated values, a regression line (n=11) is shown in (c) along with its associated statistical descriptors.
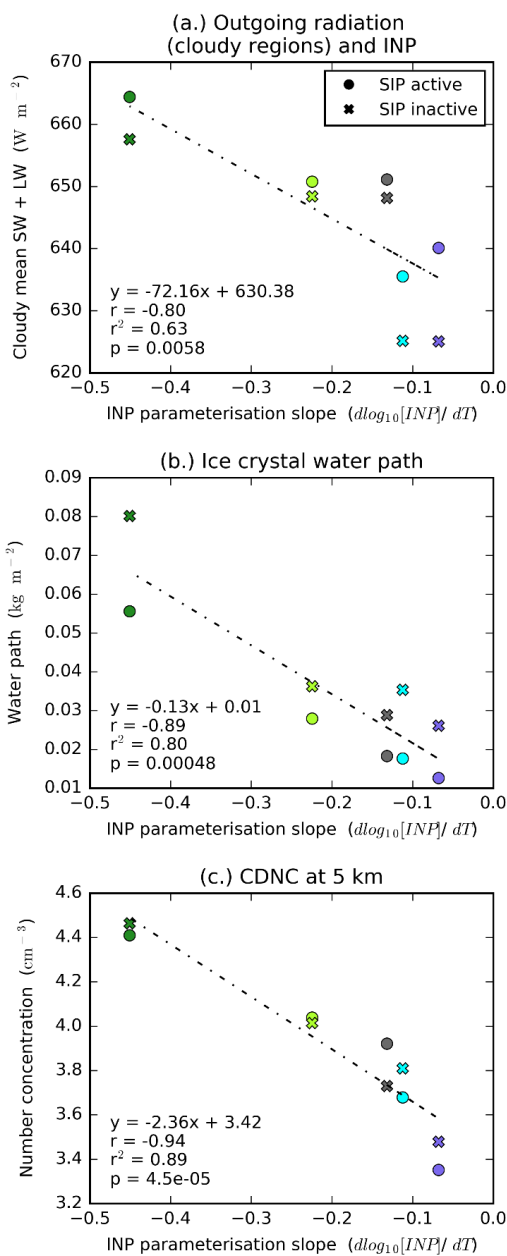
Figure 5. **Outgoing radiation from cloudy regions and INP parameterisation slope. Scatter plots of INP parameterisation slope and total daytime outgoing radiation from cloudy regions (a), in-cloud mean ice crystal water path (b), and in-cloud cloud droplet number concentrations at the start of the mixed-phase region (5 km) (c). Also shown are the respective regression lines (n=10) and associated statistical descriptors.**
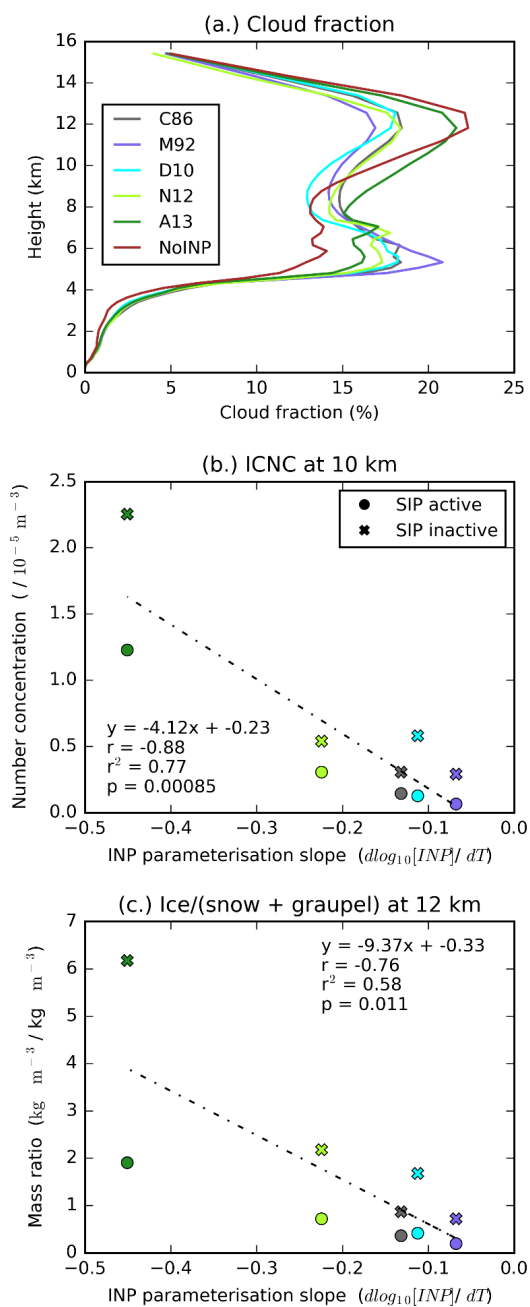
Figure 6. Cloud fraction and INP parameterisation slope. Domain-mean cloud fraction profile (a), INP parameterisation slope plotted against ice crystal number concentration at 10 km (b) and mass ratio of ice crystals to snow plus graupel at 12 km (c). Also shown in (b) and (c) are the respective regression lines (n=10) and associated statistical descriptors.
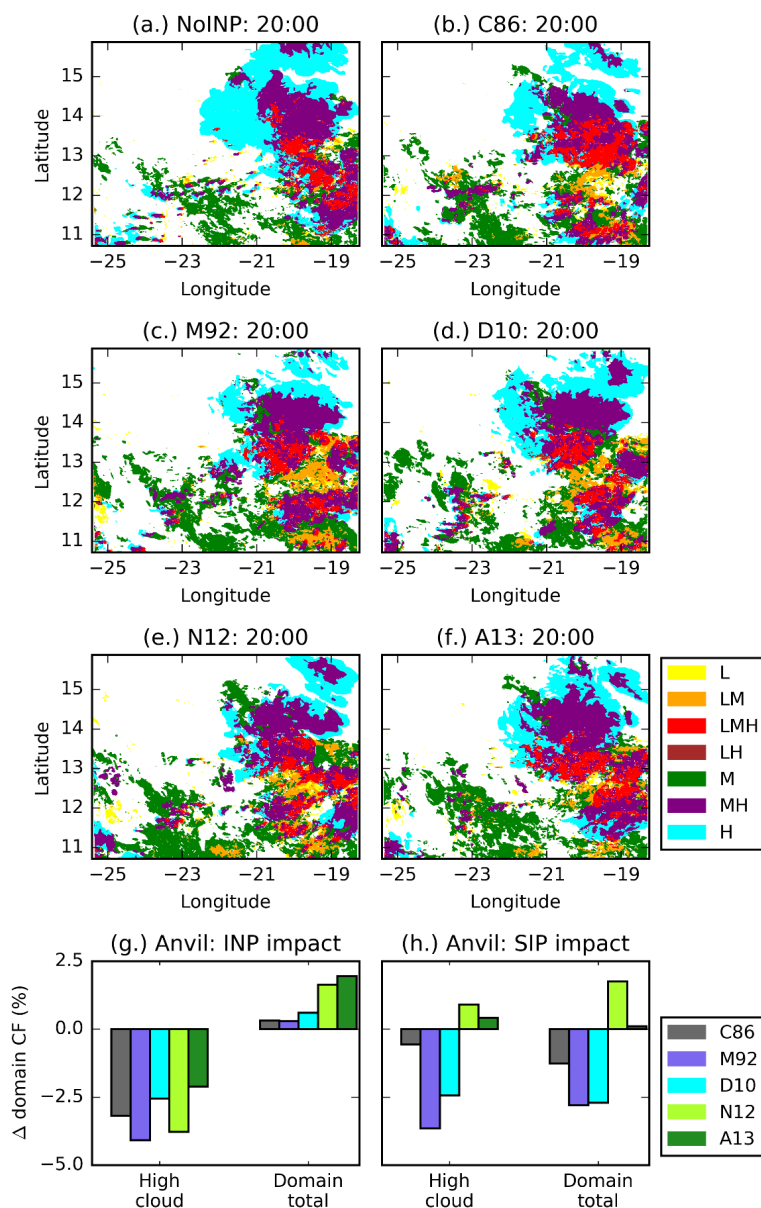
Figure 7. Vertical composition of cloud. 2D distribution of cloud type at 20:00 for all six SIP_active simulations (a-f), as well as anvil and domain cloud fraction change due to INP (g) and due to SIP (h). Clouds are categorised according to their altitude into low (L, <4 km), mid (M, 4-9 km) and high (H, >9 km) levels and mixed category columns if cloud (containing more than 10^{-5} kg kg^{-1} condensed water from cloud droplets, ice crystals, snow and graupel) was present in more than one of these levels (a more detailed description can be found in Sect. 2.1.4). A positive value in (g) or (h) indicates higher values when INP (g) or SIP (h) are active.

799 **Appendix A**

800
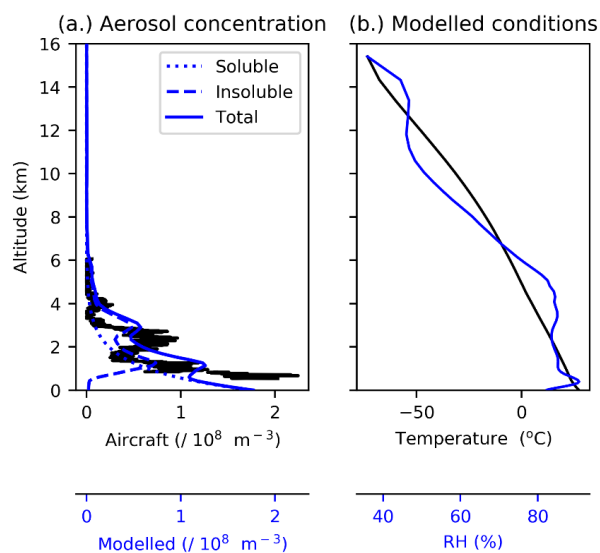
Figure A1. Observed (black line) and modelled (blue lines) aerosol concentrations (a), and modelled domain mean
temperature and relative humidity profiles (b). INP concentrations in the D10, N12 and A13 simulations are linked to the
insoluble aerosol profile shown.

804

805
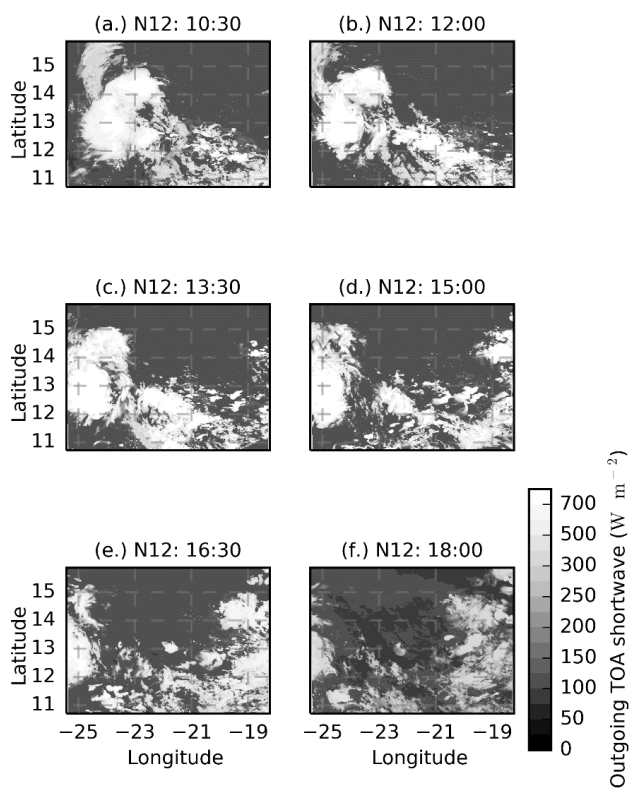
Figure A2. Cloud field evolution. Simulated top of atmosphere outgoing shortwave radiation for the N12 simulation in the daylight hours throughout the study period (a-f).
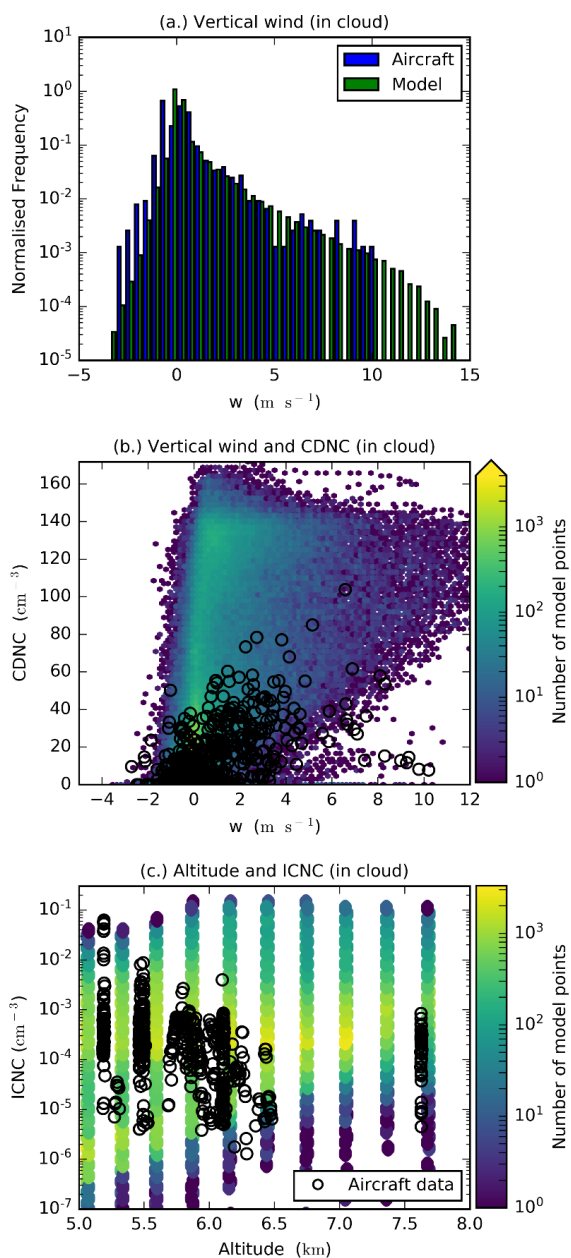
Figure A3. Comparison of observed conditions from the b933 ICED field campaign flight on the 21st August 2015 and the modelled conditions. Vertical wind speed from the model and aircraft data (a), a 2D histograms of modelled vertical wind against cloud droplet number concentration (CDNC) (b) and altitude plotted against ice crystal number concentration (ICNC) (c) with the aircraft data overlaid. Modelled values are selected from clouds between 10 and 150 km² in size from the N12 simulation.

815

816
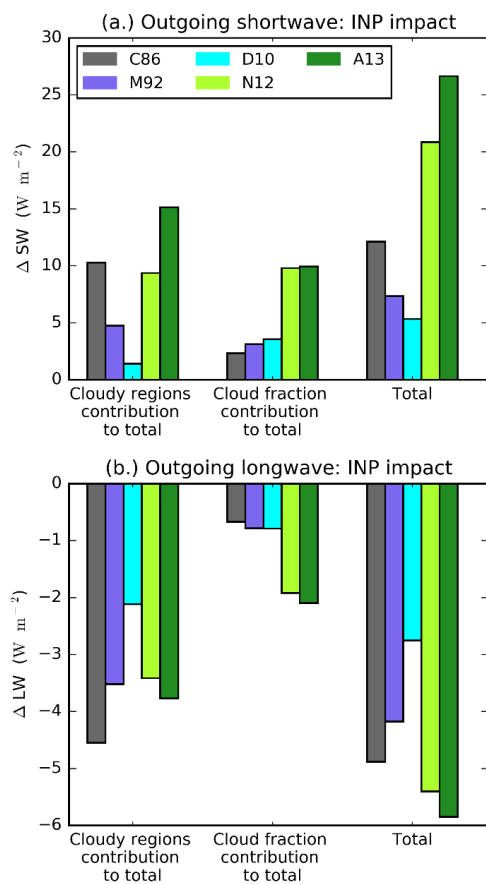
Figure A4. Effect of INP on domain mean daytime outgoing TOA shortwave and longwave radiation. The change from the NoINP simulation is shown (INP - NoINP). A positive value indicates more outgoing radiation when INP are present. The contributions of changes in outgoing radiation from cloudy regions (left) and cloud fraction (middle) to the total radiative forcing (right) are also shown.

821

822
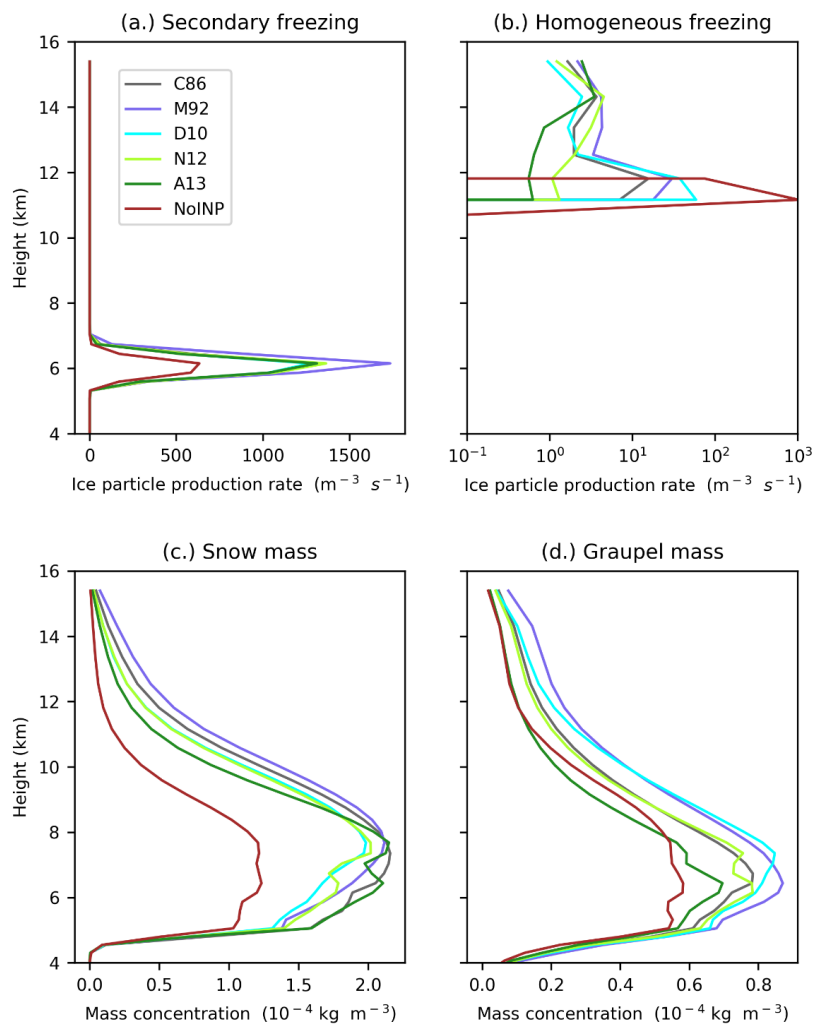
Figure A5. Profiles of some microphysical properties of the simulated clouds. Mean in-cloud ice particle production rates

from secondary (b) and homogeneous (c) freezing, snow mass concentration (c) and graupel mass concentration (d).

825

826

827
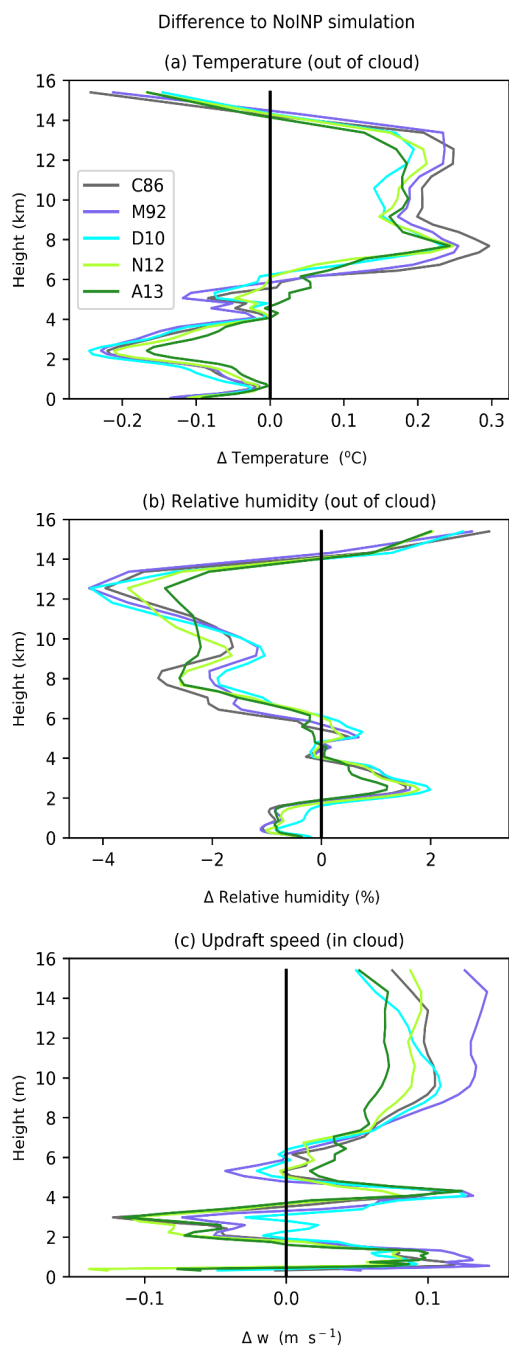
Figure A6. Effect of INP on domain mean out of cloud temperature (a) and relative humidity (b), and in cloud updraft speed (c). The difference from the NoINP simulation is shown, a positive value indicates a higher value when INP is present.